New mechanistic insights into the Claisen rearrangement of chorismate – a Unified Reaction Valley Approach study

Marek Freindorf, Yunwen Tao, Daniel Sethio, Dieter Cremer & Elfi Kraka

Taylor & Francis
Taylor & Francis Group

DIETER CREMER MEMORIAL

Check for updates

New mechanistic insights into the Claisen rearrangement of chorismate – a Unified Reaction Valley Approach study

Marek Freindorf [ORCID], Yunwen Tao, Daniel Sethio [ORCID], Dieter Cremer and Elfi Kraka [ORCID]

Computational and Theoretical Chemistry Group (CATCO), Department of Chemistry, Southern Methodist University, Dallas, TX, USA
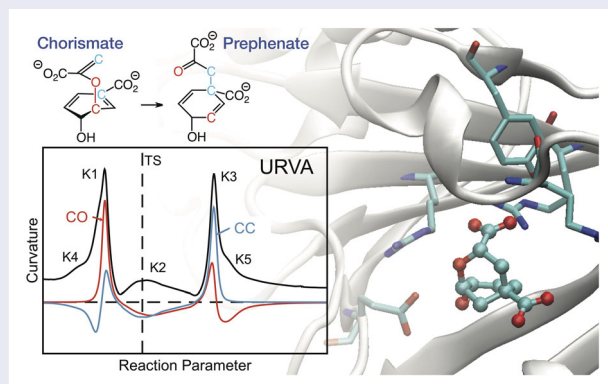
ABSTRACT

The *Bacillus subtilis* chorismate mutase catalysed Claisen rearrangement of chorismate to prephenate is one of the few pericyclic processes in biology, and as such provides a rare opportunity for understanding how Nature promotes such rearrangements so successfully. The major focus of this work is on (i) Exploring the hypothesis that the mechanism of the chorismate rearrangement is the same in the gas phase, in the aqueous solution and in the enzyme; (ii) Investigating current suggestions that the enzyme lowers the barrier via transition state stabilisation rather than via space confinement; and (iii) A comparison of Nature's way of catalysing the reaction with a gold(I) catalysed chorismate rearrangement. Based the Unified Reaction Valley Approach (URVA), for the first time, a detailed one-to-one comparison of the rearrangement in the gas phase, in the aqueous solution and in the enzyme is presented. URVA confirms that the actual chemical process of CO bond breaking and CC bond forming is the same for all media and unravels the unique catalytic function of the enzyme as a combination of shortening the process of positioning the enolpyruvyl side chain over the cyclohexadienyl ring by space confinement in concert with facilitating CO cleavage by enhanced charge polarisation. The transition state does not play a signifiant role for the rearrangement. In contrast, the gold catalyst changes the chemical process. The rearrangement is split into two steps by switching between Au[I]-π and Au[I]-σ complexation, thus avoiding the energy consuming CO breakage in the first step. Suggestions are made for metalloenzyme analogues combining both strategies.

1. Introduction

The *Bacillus subtilis* chorismate mutase (BsCM) catalysed intramolecular Claisen rearrangement of chorismate (**1**) to prephenate (**3**) (see Figure 1) is one of the few pericyclic processes in biology [1–3]. It is an important part of the *shikimate pathway* controlling the biosynthesis of aromatic amino acids (e.g. tryptophan, tyrosine, and phenylalanine) in the cells of fungi, bacteria and higher plants [4–7], and as such has become one of the most studied enzyme reactions [8–32]. The theoretical interest in the BsCM-catalysed chorismate rearrangement was triggered by the fact that (i) the substrate does not covalently bind to the active site [33–35] so that the system can be easily separated into a QM region (the substrate)
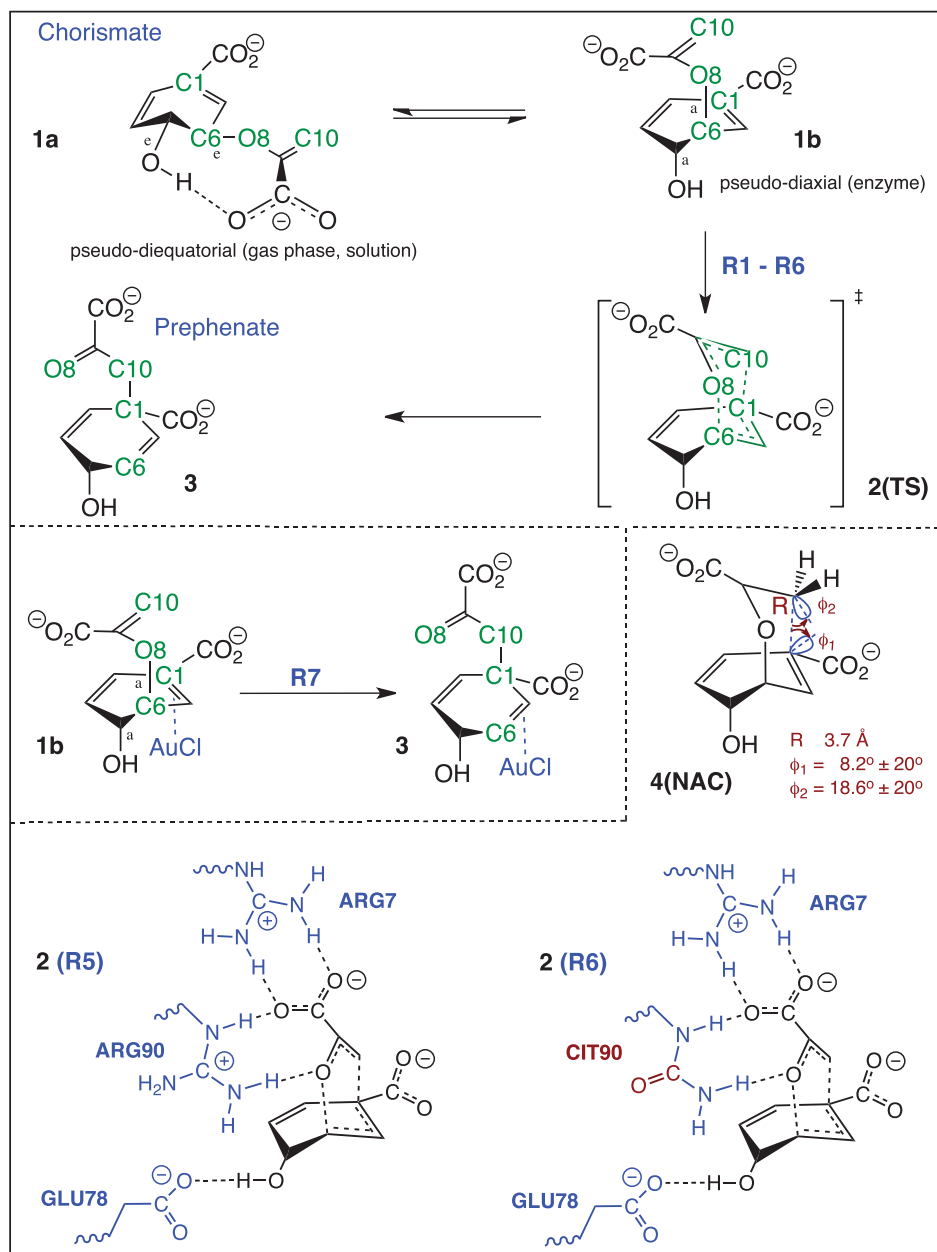
Figure 1. Claisen rearrangement of chorismate to prephenate; **R1**: gas phase reaction, **R2**: reaction in aqueous solution modelled with PCM, **R3**: reaction in aqueous solution modelled with TIP3P, **R4**: enzyme reaction, QM part: chorismate, MM part: BsCM, **R5**: enzyme reaction, QM part: chorismate and ARG7, ARG90, and GLU78, MM part: remaining BsCM, **R6**: enzyme reaction, QM part: chorismate, MM part: BsCM with ARG90 exchanged to CIT90, **R7**: gas phase reaction catalysed by AuCl. Molecule **4**, definition of the near attack conformers (NACs).

and an MM region (the enzyme); and (ii) the wealth of experimental data available to cross-check the reliability of the computational studies [2, 36–45].

Site-directed mutagenesis including X-ray structure analysis [40, 44, 46–50], kinetic studies [50], as well as calculations [19, 26, 51–55] have suggested that the decisive factor of the BsCM catalysis leading to a 2×10^6 acceleration of the conversion of **1b** to **3** is transition state (TS) stabilisation with a cationic enzyme residue, either an arginine or a lysine proximal to the ether oxygen of the substrate [33, 56]. Studies of the changes in the heat capacity upon complexation suggest that enzyme binding to the substrate **1** is relatively weak while that to the TS is relatively strong [57]. Recently, Burschowsky and co-workers provided evidence for TS stabilising via electrostatic and H-bonding enzyme-substrate interactions based on a density functional study [43]. This supports the theory that the BsCM catalysis is not

driven by shape complementarity to the substrate, but as already introduced by Pauling seven decades ago [58] that an enzyme is designed to bind and stabilise the TS.

In contrast, other studies emphasise the importance of so-called near attack conformers (NACs), which have already a structure close to that of the TS (**2**) [20, 59, 60]. According to Hur and co-workers [61–63], BsCM speeds up the Claisen rearrangement by binding the chorismate primarily in its NAC form, rather than by stabilising the TS. However, QM/MM simulations of Bruice and co-workers [64] showed that the NACs structures for the Claisen rearrangements and their charge distributions in the gas phase, in water, and in the enzyme do not support significant electrostatic stabilisation of **2**. The charge distributions of the NACs and **2** in the enzymatic reaction differ only gradually and can account for only 10% of the efficiency of the enzymatic reaction. This is in line with other studies concluding that NACs only moderately contribute to the catalytic power [23, 59]. One has also to consider that there is no unique way of defining NAC structures in contrast to **2** which is a well-defined stationary point on the potential energy surface. Therefore, the definition of the NACs **4** (see Figure 1), may bias the results [53, 65, 66]. Strain and conformational compression of the substrate at the enzyme active site were also proposed to explain the rate acceleration by BsCM [26], however could not be identified as key factor [22, 23].

Over decades the modelling of chemical reactions has proved that simplifications of the physical reality are an important tool to guarantee progress in elucidating the reaction mechanism. Clearly, the importance of free-energy landscapes for enzyme catalysis [67] is non-disputable, but in view of the difficulties of evaluating a free-energy surface for a complex enzymatic reaction and overemphasising the protein dynamics as key factor for catalysis, Warshel [68] has pointed out that there has not yet been any study that consistently established a connection between an enzyme's conformational dynamics and a significant increase in the catalytic contribution of the chemical step. He advocates that mechanistic insights can also be gained by the investigation of the potential energy surface describing enzyme and substrate interactions under environmental influences. This holds in particular if the reaction under study is not predominantly entropy driven, which applies to the chorismate rearrangement [69] and if one is primarily interested in the electronic structure changes that drive the reaction mechanism. Following this path, we have provided in many investigations sufficient evidence that the analysis of an energetically preferred reaction path can be generalised to a large extent, providing detailed insights into the mechanism of families of reactions, stretching from organic reactions to homogenous catalysis [70–76]. In this work, we will provide the proof of concept that this also holds for enzymatic reactions.

The major objectives of this study are the following: (i) Prove/disprove the hypothesis that the mechanism of chorismate rearrangement is the same in gas phase, solution and enzyme, e.g. space confinement does not play a major role; (ii) Test the current suggestions that the enzyme lowers the barrier via TS stabilisation, e.g. electrostatic and H-bonding interactions preferentially between the migrating ether oxygen and Arg90 of the enzyme; (iii) Investigate the overall importance of the TS for the rearrangement; (iv) Compare the enzyme catalysis with a Au(I) catalysed chorismate rearrangement. Based on the findings obtained in this work suggestions for BsCM analogues are made.

For this purpose, we investigated the Claisen rearrangement of chorismate in different environments as summarised in Figure 1; (i) *gas phase*: **R1**; (ii) *aqueous solution*: **R2**: describing the solvent effects via a polarised continuum model (PCM); **R3**: describing the solvent effects via a QM/MM approach in order to consider individual solute–solvent interactions; (iii) *reaction in BsCM*: **R4**: QM/MM approach, QM part: chorismate, MM part: BsCM; **R5**: QM part: chorismate plus side chains of Arg90, Arg7 and Glu78 of BsCM in order to explicitly describe the influence of enzyme-substrate hydrogen bonding, MM part: remaining BsCM atoms, **R6**: QM part: chorismate, MM part: BsCM with Arg90 exchanged to Cit90; (iv) *Gold(I) catalysis*: **R7**: gas phase reaction catalysed by AuCl. The manuscript is structured in the following. In Section 2, we briefly describe the quantum chemical methods and tools used in this work to investigate reactions **R1**–**R7**. Results are discussed in Section 3, and in Section 4, we will draw the conclusions of this investigation including an outlook on how the results of this work can be applied to future *De Novo* metalloenzyme catalyst design.

2. Computational methods

Two special tools were applied in this study, the *Unified Reaction Valley Approach* (URVA) [77, 78] and the *Local Mode Analysis* of Konkoli and Cremer [79–84], which will be briefly introduced in the following.

URVA characterises the reaction complex (RC, e.g. the union of reacting molecules) as it moves along the reaction path on the potential energy surface (PES) from the entrance channel up to the TS and down into the exit channel. The key feature of URVA is the analysis of the reaction path curvature. Moving along the reaction path, any electronic structure change of the RC is

registered by its vibrations. The change in the vibrations in turn leads to a change in their coupling with the translational motion along the reaction path. Following the *Reaction Path Hamiltonian* approach of Handy, Miller, and Adams [85], which spans the reaction valley via the translational motion along the path and molecular vibrations perpendicular to it, we calculate at each path point s the vibrational–translational coupling via the so-called curvature coupling coefficients $B_{\mu,s}(s)$ [77, 78, 85]. These coefficients define the scalar reaction path curvature $\kappa(s)$ [77, 78, 85], which means that the curvature of the reaction path directly reflects the changes in the electronic structure of the RC during the chemical reaction. Each chemical event (e.g. bond breakage/formation, rehybridisation, or charge transfer and charge polarisation, etc.) corresponds to a local curvature maximum Km flanked by two curvature minima Mn, e.g. locations with minimal change of the RC. The curvature minima can often be classified as *Hidden Intermediates* [86, 87], which can become real intermediates if the reaction is changed, e.g. by addition of functional groups, adding a catalyst, or changing the environmental conditions [70–76]. Kraka and Cremer coined the reaction path region from one curvature minimum to the next embedding a curvature maximum a *reaction phase* [86, 87]. Different chemical reactions possess different curvature patterns with a different number of reaction phases, which can be used as their fingerprints. Further reaction details, such as which part of the RC changes in which reaction phase, are obtained from decomposition of the scalar reaction path curvature $\kappa(s)$ into internal coordinate contributions [77]. The analysis of $\kappa(s)$ in terms of bond length, bond angle, and dihedral angle components can be complemented by a decomposition into Cremer–Pople puckering coordinates [88]. In this way, the conformational changes of cyclic or pericyclic reactions can be quantitatively monitored [70, 73, 89]. The URVA analysis has been successfully applied to organic and homogeneous catalysis reactions (see, for example references [70–76]). In this work, we applied URVA for the first time to an enzyme reaction. It is an important advantage of the URVA analysis that different reactions can be directly compared, which otherwise would only be possible for the stationary points on the potential energy surface [89].

Besides providing important information about the electronic structure change during the course of a chemical reaction, vibrational spectroscopy can also serve as a valuable source for a quantitative assessment of the intrinsic strength of a chemical bond. However, the use of normal vibrational modes is of limited use for this purpose. Normal vibrational modes are generally delocalised caused by electronic and mass-coupling [90]. Therefore,

accurate bond strength descriptors are only obtained when referring to localised rather than delocalised vibrational modes. The electronic coupling is suppressed by solving the Wilson equation [90], which involves a diagonalisation of the force constant matrix. Konkoli and Cremer showed that the remaining mass (kinematic) coupling can be eliminated by solving a mass-decoupled equivalent of the Wilson equation, leading to local vibrational modes, which are associated with internal coordinates q_n such as bond length, bond angle, and dihedral angle [79, 80]. Zou and Cremer verified that there is a one-to-one relationship between the local and the normal vibrational mode through an adiabatic connection scheme (ACS) [83] and they recently demonstrated that there is a direct relationship between the local stretching force constant k^a of a chemical bond and its intrinsic strength [91]. Therefore, the local stretching force constant k^a is an ideal bond strength measure, which has been successfully applied to covalent bonds [92–100] and non-covalent [101–117] interactions. In this work, we used the Local Mode Analysis for a quantitative assessment of enzyme-substrate H-bonding and of the initial strength of the CO bond to be broken during the chorismate rearrangement.

To simplify comparison, the local mode force constants k^as were converted to relative bond strength orders (*BSO*) n by utilising an extended Badger rule according to which *BSO* n is related to the local stretching force constant k^a via the following power relationship [118]:

$$BSO\ n = A(k^a)^B$$

The coefficients A and B are fully determined by two reference values and the requirement that for a zero-force constant *BSO* n becomes zero. We used in this work the following references: (i) *Hydrogen bonds*: FH, $n = 1$ and F_2H^-, $n = 0.5$ leading to $A = 0.50437$ and $B = 0.30648$; (ii) *CO bonds*: CH_3OH, $n = 1$ and CH_2O, $n = 2$ leading to $A = 0.35658$ and $B = 0.66679$; (iii) *CC bonds*: C_2H_6, $n = 1$ and C_2H_4, $n = 2$ leading to $A = 0.32519$ and $B = 0.80129$.

The reaction valley was evaluated at the B3LYP density functional level [119, 120] with Pople's $6\text{-}31 + G(d, p)$ basis set [121–123] for reactions **R1** and **R2** and the QM part of reactions **R3–R6**. We decided for B3LYP, because this functional provides a reliable description of the chorismate rearrangement [21] and, therefore was also used in other chorismate studies [33, 43, 124, 125]. The density functional integrations were performed with an ultrafine grid [126] and a tight convergence criterion. The aqueous solution was represented in reaction **R2** by the polarisable continuum solvent model (PCM) of Tomasi and co-workers [127] and in reaction **R3** via a QM/MM

approach. The QM part included chorismate, which was surrounded by a TIP3P water sphere [128] of a radius 20 Å, with an external harmonic potential of a force constant 10 kcal/mol/Å^2 defining the MM part. MM parameters were taken from the AMBER General Force Field for organic molecules [129]. Initial equilibration of the solvent was done by molecular dynamics (2000 steps of minimisation, 100 ps heating from 0 to 300 K, followed by production dynamics for 2 ns). The following annealing dynamics was performed for 200 ps by short-time heating the system to 500 K and long-time cooling to 0 K. All simulations were performed with a constrained geometry of the solute with a force constant 1500 kcal/mol/Å^2. The QM part in reaction **R4** included the chorismate and the MM part all BsCM atoms. The initial protein coordinates were taken from the crystal structure of the Arg90Cit (citrulline) mutation of BsCM in complexation with a transition state analogue [44]. The Arg90Cit mutation was manually replaced back to the original Arg90 structure. The MM parameters were taken from AMBER General Force Field for organic molecules [129]. For neutralisation, six sodium counter ions were used, based on the electrostatic potential. The entire protein was minimised at the MM level with a fixed TS geometry. The following QM/MM calculations were performed without any geometry constraints allowing both the enzyme and substrate to relax to their optimal conformation. The QM part of reaction **R5** included chorismate and the side chains of Arg90, Arg7 and Glu78 (which were identified by several authors as most important for the rearrangement process [18, 23, 33, 130]), while the MM part included the remaining enzyme atoms. This restriction kept the QM/MM evaluation of the complete IRC including the evaluation of second derivatives at each path point practicable. Reaction **R6** was composed of chorismate QM part and the original Arg90Cit mutation of BsCM [44]. Both steps of reaction **R7** were calculated in the gas phase using the B3LYP/6 − 31 + G(d, p) /SDD level of theory and the Stuttgard-Dresden effective core potential (SDD) [131] with a corresponding basis set for the Au atom [132].

We used as reaction path the intrinsic reaction coordinate (IRC) path of Fukui [133], which was determined with a step size of $s = 0.03$ amu$^{1/2}$ Bohr applying the improved reaction path following procedure of Hratchian and Kraka, allowing to follow a chemical reaction far out into entrance and exit channel [134]. The URVA and Local Mode analyses were carried out with the program COLOGNE18 [135]. The DFT calculations were carried out with Gaussian09 [136], the molecular dynamics simulations with AMBER 14 [137], and the Natural Bond Orbital (NBO) charges were calculated with the program NBO 6 [138, 139].

3. Results and discussion

In the following, the results from this work are presented. First, the energetics of the reactions **R1**–**R6** are summarised, followed by the URVA analysis of the reaction path curvature and path direction including a discussion of the energy contribution to the reaction barrier to each of the reaction phase. This is complemented by a ring puckering analysis and the examination of the impact of charge transfer and polarisation as well as enzyme-chorismate H-bonding on the BsCM-catalysed chorismate rearrangement. In the last section, the enzyme catalysis is compared with the gold(I) catalysis.

Reaction energetics. In Table 1 and Figure 2, the energetics of reactions **R1**–**R6** are presented. The non-catalysed gas phase reaction **R1** has an activation energy $\Delta E^{\ddagger}$ of 24.4 kcal/mol (activation enthalpy $\Delta H^{\ddagger}$: 22.8 kcal/mol) and a reaction energy ΔE_R of −23.7 kcal/mol (reaction enthalpy ΔH_R : −23.7 kcal/mol). In aqueous solution described by PCM (reaction **R2**) $\Delta E^{\ddagger}$ is lowered by 4.7 kcal/mol ($\Delta H^{\ddagger}$ by 4.6 kcal/mol) and the exothermicity is slightly reduced (ΔE_R by 1.4 kcal/mol and ΔH_R by 1.5 kcal/mol). A more accurate description of water via a QM/MM approach using TIP3P (reaction **R3**) leads to a further lowering of the $\Delta E^{\ddagger}$ to a value of 17.3 kcal/mol ($\Delta E^{\ddagger}$ 16.3 kcal/mol) and to the corresponding ΔE_R value of −18.1 kcal/mol (ΔH_R − 18.3 kcal/mol). These results suggest that a polar medium facilitates the rearrangement in line with studies of Jorgensen and co-workers [140] and of Karplus

Table 1. Energetics of the Claisen rearrangement of **1**–**3** in different environments.

Reaction	$\Delta E^{\ddagger}$	$\Delta H^{\ddagger}$	ΔE_R	ΔH_R
(1b→3)				
R1 Gas phase	24.4	22.8	−23.7	−23.7
R2 PCM	19.7	18.2	−22.3	−22.2
R3 TIP3P	17.3	16.3	−18.1	−18.3
R4 BsCM	11.6	10.7	−15.2	−14.9
R5 BsCM$_{ext}$	10.4	8.3	−17.0	−16.6
R6 BsCM$_{mut}$	14.9	13.0	−11.0	−11.4
(1a→1b)				
R1 Gas phase	12.2	11.6	11.9	12.0
R2 PCM	8.3	7.9	7.2	7.4
R3 TIP3P	4.8	4.9	3.7	4.4
(1a→3)				
R1 Gas phase	37.5	36.0	−10.5	−10.5
R2 PCM	26.9	25.6	−15.1	−14.8
R3 TIP3P	21.0	20.6	−14.4	−13.9
R5 BsCM$_{ext}$[a]	14.4	12.7	−13.3	−12.2
Exp: Water		20.7 ± 0.4[b]		
Exp: BsCM		12.7 ± 0.4[b]		−13.2 ± 0.5[c]

Note: B3LYP density functional level of theory [119, 120] with Pople's 6 − 31 + G(d, p) basis set [121–123] for reactions **R1** and **R2** and the QM part of reactions **R3**–**R6**. Representation of aqueous solution: in reaction **R2** by the PCM model [127]; in reaction **R3** via a QM/MM approach using TIP3P [128] for the MM part. MM part of **R4**–**R6**: AMBER [129]. All values in kcal/mol.
[a] (**1a → 3**) part taken from TIP3P, see text.
[b] Experimental data from [36, 69].
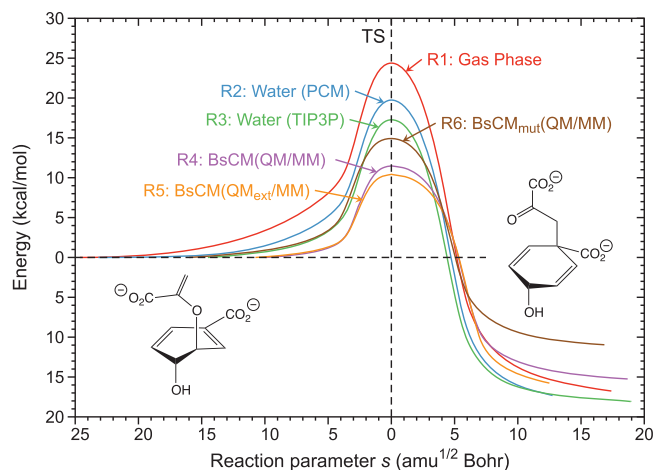[c] Experimental data from [50].

Figure 2. Energy profile of the chorismate rearrangements in the gas phase (**R1**), aqueous solution modelled with PCM (**R2**), modelled with TIP3P (**R3**), in BsCM (**R4**), in BsCM with an extended QM part(**R5**), and in mutated BsCM (**R6**). B3LYP/$6 − 31 + G(d, p)$ calculations.

and co-workers [52]. From a technical point of view, it is important to note that a polarisable continuum model is obviously not sufficient to fully account for these effects. For the BsCM-catalysed reaction **R4**, we find $\Delta E^{\ddagger}$ and $\Delta H^{\ddagger}$ values of 11.6 and 10.7 kcal/mol and ΔE_R and ΔH_R values of −15.2 and −14.9 kcal/mol, respectively. Increasing the QM part, (reaction **R5**) lowers the barriers ($\Delta E^{\ddagger}$ by 1.2 kcal/mol and $\Delta H^{\ddagger}$ by 2.4 kcal/mol) as well as the exothermicity (ΔE_R by 1.8 kcal/mol and ΔH_R by 1.7 kcal/mol) showing the importance of enzyme-substrate H-bonding. Replacing Arg90 with Cit (reaction **R6**) moves the energetics back to higher barriers, $\Delta E^{\ddagger} = 14.9$ kcal/mol and $\Delta H^{\ddagger} = 13.0$ kcal/mol confirming that the charged Arg90 plays a role for the enzyme catalysis. In summary, the lowering of the activation enthalpy by 14.5 kcal/mol in comparison with the gas phase reaction reflects the catalytic power of the enzyme.

The calculated activation and reaction enthalpies cannot directly be compared with the available experimental data. One has first to consider how the experiments were conducted and then to adjust the calculated values accordingly, which sometimes has been overlooked. The experimental activation enthalpies $\Delta H^{\ddagger}_{exp}$ for the rearrangement of **1**–**3** in water and in BsCM were obtained by measuring the disappearance of **1** in aqueous solution at different temperatures in the presence and absence of BsCM [36, 69]. The actual concentration of **1** was monitored spectrophotometrically at 274 nm and converted to thermodynamic data using the (first-order) Michaelis-Menten equation [69]. In this way, $\Delta H^{\ddagger}_{exp} = 20.7 \pm 0.4$ kcal/mol was derived for the rearrangement in water and $\Delta H^{\ddagger}_{exp} = 12.7 \pm 0.4$ kcal/mol for the reaction in

the presence of BsCM [36, 69]. The pseudo-diequatorial conformation (**1a**) has been confirmed as the global minimum in water and the pseudo-diaxial form (**1b**) as the active conformation that performs the Claisen rearrangement (see Figure 1), and the form which binds to enzyme [33, 141–144]. These findings are confirmed by our calculations as shown in Table 1. In addition, all our attempts to obtain a stable complex between BsCM and **1a** failed revealing that the enzyme is designed to host the active form **1b**. This implies that the transformation of **1a**–**1b** occurs in the aqueous solution, and that therefore the measured data describe the reaction (**1a** → **3**). Taking this into account and adjusting our calculated (**1b** → **3**) reactions accordingly, we obtained a $\Delta H^{\ddagger}$ value for the aqueous reaction **R3** of 20.6 kcal/mol close to the experimental value of 20.7 ± 0.4 kcal/mol and a $\Delta H^{\ddagger}$ value of 12.7 kcal/mol matching the experimental value of 12.7 ± 0.4 kcal/mol. The experimental reaction enthalpy of the chorismate rearrangement was derived using using micro-calorimetry and high-performance liquid chromatography [50], leading to a value of ΔH_R of −13.2 kcal/mol at 298 K, which is in good agreement with our calculated value of −12.2 kcal/mol. Measured entropy contributions to the free-energy barrier in both BsCM and in aqueous solution turned out to be small and similar ($\Delta S^{\ddagger}_{exp.} = -9.1 \pm 1.2$ and -12.1 ± 0.4 kcal/mol for BsCM and water, respectively), supporting the arguments that BsCM catalysis is an enthalpic effect [31, 69]. Therefore, we exclude an entropy discussion from the current work.

The energetics allow to test the overall performance of a catalyst; however, they do not provide a detailed insight into the electronic/steric factors determining the overall enzyme efficiency, given the fact that the energy is a cumulative property in its nature. To learn more about the mechanistic details, we will focus in the following section on the analysis of the reaction path curvature.

Curvature profiles and reaction mechanism. The analysis of the reaction path curvature and its decomposition into internal coordinate components presents a unique way of quantifying the mechanism of a chemical reaction. In Figure 3, the curvature profiles for reactions **R1**–**R6** and their decomposition into the most important components are shown. Videos following the evolution of the RC along the reaction path are provided for reactions **R1**–**R4** and reaction **R6** in the online supplemental data.

An inspection of the curvature profiles shown in Figure 3 and the corresponding data in Table 2 reveals that all reactions are characterised by two distinct curvature peaks K1 and K3, separated by a small curvature enhancement K2 and being located in the chemical phases 3–5 (highlighted with a grey bar in Figure 3). The actual chemical process of C6O8 bond cleavage and
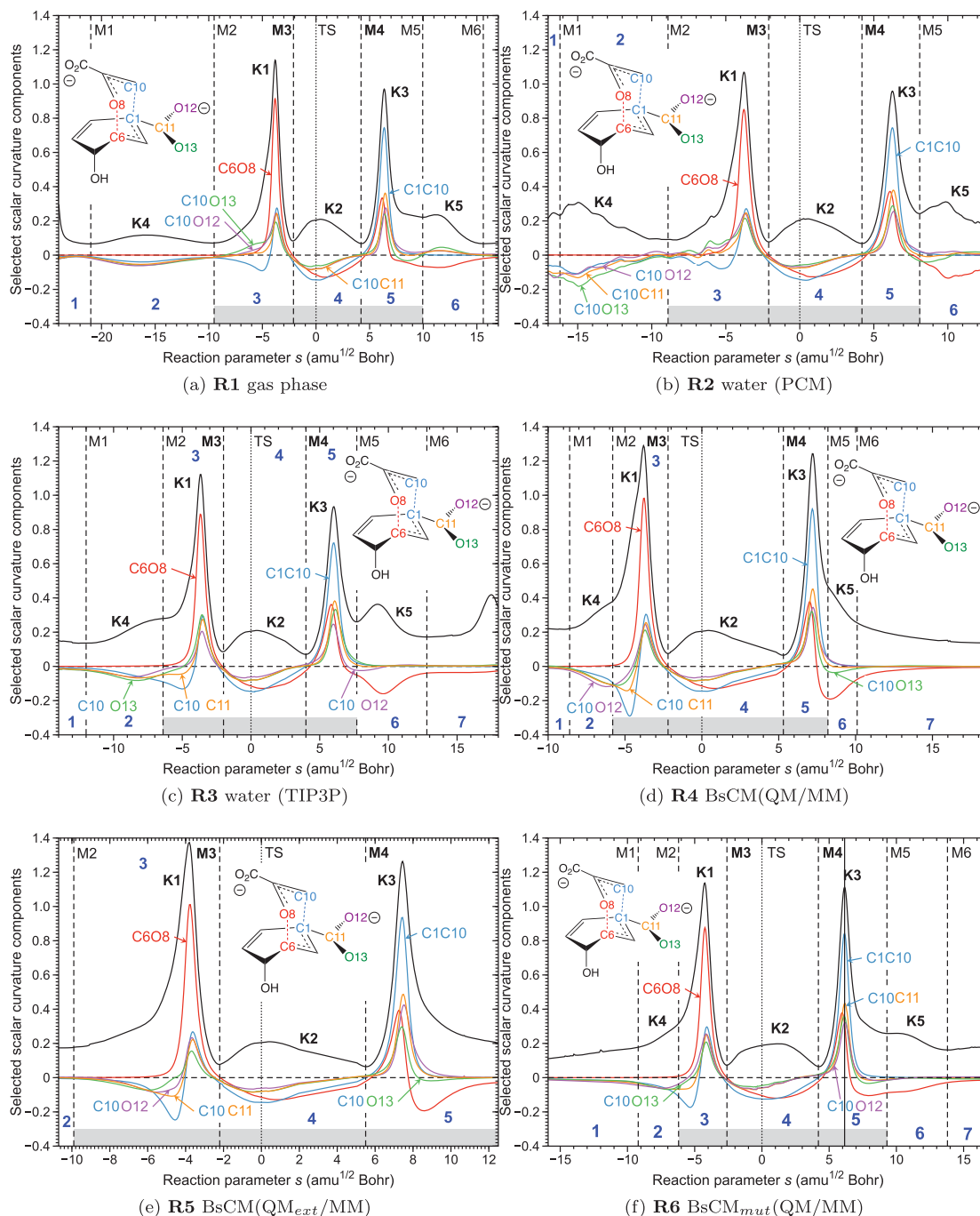
Figure 3. Scalar curvature as a function of the reaction path parameter s (solid black line) for the chorismate rearrangements **R1**–**R6**. The decomposition of the scalar curvature into the most important components is given. The borders of the reaction phases are indicated by vertical dashed lines at curvature minima M1, M2, M3, etc. Curvature maxima are indicated by K1, K2, K3, etc. The TS at $s = 0$ amu$^{1/2}$ Bohr is also indicated by a vertical dotted line. The reaction phases are denoted and the chemical phases are highlighted with a grey bar.

C1C10 formation follows a similar pattern for all six reactions studied in this work, in line with the suggestion that the mechanism of the chorismate rearrangement should be the same in gas phase, solution, and in the enzyme, made by several authors [33, 144]. In phase 3, the most energy consuming part of the reaction starts, e.g. the cleavage of the C6O8 bond, characterised by curvature peak K1. This peak is dominated by the C6O8

contribution (see, Figure 3) accompanied by a small resisting contribution of C1C10 (see, Figure 3), the new bond to be formed. In the following phase 4, stretching from M3 to M4 and containing the TS, reorganisation of the electronic structure for the finalisation of bond cleavage and formation takes places, which leads to resisting contributions from C6O8 and C1C10. The finalisation of the formation of the new C1C10 bond and final breaking

Table 2. Characterization of the reaction path curvature profiles of the Claisen rearrangement **R1**–**R6** in terms of curvature peaks and curvature minima. All path points and distances are given in s units ($amu^{1/2}$ Bohr). For a description of symbols see Figure 3.

Reaction	s(K1)	s(K3)	K3/K1[a]	Δs(TS)[b]	s(M3)	s(M4)
R1	−3.81	6.36	85	−1.4	−2.1	4.2
R2	−3.78	6.27	89	−1.3	−2.1	4.2
R3	−3.64	6.04	83	−1.2	−2.0	4.0
R4	−3.80	7.08	99	−1.7	−2.2	5.3
R5	−3.80	7.45	92	−1.8	−2.2	5.5
R6	−4.25	6.15	98	−1.0	−2.6	4.2
Reaction	[K1,K3][c]	[M3,M4][d]	[M2,M5][e]	[M2,K1][f]	[M1,M2][g]	
R1	10.2	6.3	19.5	5.7	11.5	
R2	10.1	6.3	17.0	5.1	7.3	
R3	9.7	6.0	14.1	2.7	5.6	
R4	10.9	7.5	14.0	2.0	2.8	
R5	11.3	7.7	29.0[h]	6.1	–	
R6	10.4	6.8	15.5	1.9	3.0	

[a] Ratio of the curvature peak K3 (breaking of the C6O8 bond) and K1 (forming of the C1C10 bond) in percent.
[b] Shift of the position of the TS from the centre of [K1,K3], the negative sign denotes a shift into the entrance channel, (early transition state).
[c] s range between K1 and K3.
[d] s range between M3 and M4.
[e] chemical phases.
[f] s range between M2 and K1.
[g] s range between M1 and M2.
[h] s range between M2 and last path point.

of the C6O8 bond occurs after the TS in phase 5, being characterised by curvature peak K3, which is composed of a larger C1C10 and a smaller C6O8 component, both being positive, i.e. supporting. The similarity of the actual bond breaking/forming process can be quantified with the data in Table 2. For all reactions, the curvature peaks K1 and K3 span between 10 and 11 s-units, the ratio of K3/K1 lies between 83% and 98%, and the range between M3 and M4 is around 6–8 s units. The position of the TS is always closer to K1 than K3 (see negative shift values $s(\Delta(TS)$ in Table 2) e.g. the reaction is characterised by an early TS and the actual bond breaking and bond forming processes are asynchronous as speculated by several authors [54, 124, 145–147]. Noteworthy is that the TS does not play any signifiant mechanistic role as reflected by the small curvature enhancement K2, the actual chemical process starts before the TS with the cleavage of the C6O8 bond in phase 3. The curvature minima M2 and M3 are mechanistically important as they may serve as starting points for breaking up the reaction into two steps as discussed for the gold(I) catalysis.

The striking similarity of the curvature profiles between the peaks K1 and K3 raises the question, where does the difference between reactions **R1** and **R6** come from? As obvious from Figure 3 and Table 2, the s-range covered by the entire chemical phases 3–5 is quite different, stretching from 14 to almost 30 s units (entry [M2,M5] in Table 2). Even more pronounced are differences in the pre- and post-chemical phases. The pre-chemical phase 2 becomes shorter; 7.3 s units in the

case of **R2**, 5.6 s units in the case of **R3** compared with 11.5 s units for the gas phase reaction **R1**, e.g. the water environment helps to bring the enolpyruvyl side chain of **1b** into a better position for the rearrangement reaction. The enzyme catalysed reaction **R4** (Figure 3(d)) has a short pre-chemical phase 2 of 2.8 s units, e.g. the enzyme forces **1b** into the right conformation for starting the bond breakage and the corresponding curvature peak K4 appears only as a small shoulder. In the enzyme reaction **R5** with an improved description of enzyme-substrate binding via H-bonding, there is no longer a pre-chemical phase 2 and no curvature peak K4, e.g. docked into the enzyme the enolpyruvyl side chain of **1b** is already in an optimal position over the cyclohexadienyl part to start theisomerisation reaction right away. This clearly shows that space confinement is one of the key features of the BsCM catalysis. Substitution of Arg90 with Cit, (reaction **R6**) leads again to a pre-chemical phase 2 of 3.0 s units with a small K4 shoulder (Figure 3(f)), reflecting the important role of Arg90, which will be further discussed below with regard to charge transfer and polarisation. The same trend applies for the post-chemical phases, which are related to bringing **3** into the right position for optimum ϕ-delocalisation. In **R4** the corresponding curvature peak K5 is just a small shoulder and in **R5** the post-chemical phase 6 completed absorbed by the chemical phase.

Space confinement and bond length changes: Further insights are obtained by the inspection of the C6O8 and C1C10 distances, as they evolve along the reaction path, which is presented in Figure 4. In the entrance channel, the atoms C1 and C10 have to move together to from the new CC bond. **1b** is most flexible in the gas phase, adapting a structure which keeps the two negatively charged carboxylate groups apart. This leads to the largest C1C10 distance of 3.8 Å found for all **1b** molecules investigated in this study. The enolpyruvyl side chain has to bend over towards the cyclohexadienyl ring, which stretches over a large s range (see reaction video for **R1** in the online supplemental data). In the aqueous solution, the enolpyruvyl side chain is already closer to the cyclohexadienyl ring leading to a C1C10 distance of 3.3 Å, and confined in the enzyme, the C1C10 distance of **1b** is 3.1 Å, see Figure 4(a). It is noteworthy that at curvature peak K1, the C1C10 distance becomes almost the same for all RCs, and that around curvature peak K3 the final C1C10 distance is reached for all six reactions, again confirming the similarity of the bond breaking/forming process for the gas phase reaction and the reactions in aqueous solution and in the enzyme. A complementary picture is obtained for the C6O8 bond to be broken, as shown in Figure 4(b). The C6O8 bond length stays fairly constant in all RCs until at peak K1 the C6O8 bond rupture
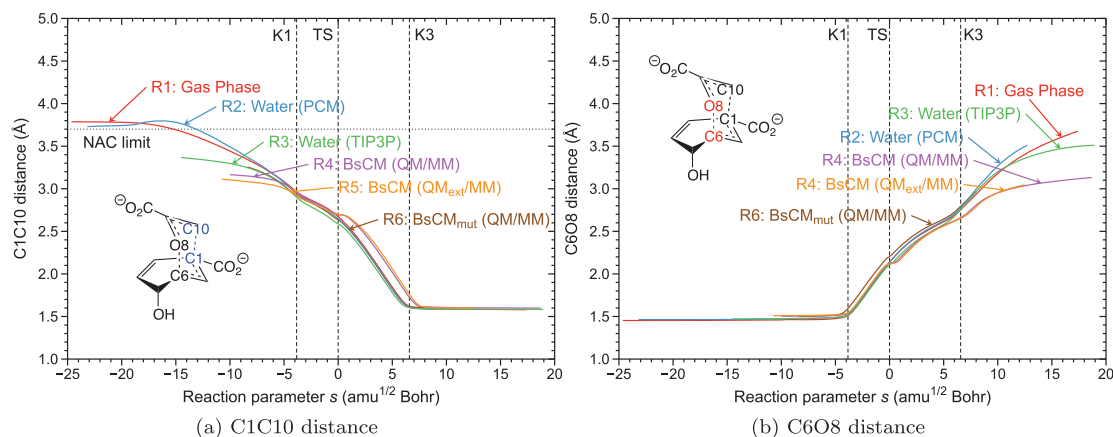
Figure 4. (a) C1C10 distance as a function of the reaction parameter s for reactions **R1**–**R6**; **(b)** C6O8 distance as a function of the reaction parameter s for reactions **R1**–**R6**. The average positions of K1 and K3 for reactions **R1**–**R6**, as well as the TS at $s = 0$ amu$^{1/2}$ Bohr are indicated by a vertical dashed line. The dotted horizontal line in Figure 4(a) denotes the NAC distance limit.

starts. Again, changes of the C6O8 distance between K1 and K3 occur with the same rate of change. However, after K3 (finalization of CO bond breakage) the C6O8 distances drift apart reflecting the different media. This fully confirms our finding that for all six reactions, the core chemical region between K1 and K3 is the same, and that space confinement determines the differences in pre- and post-chemical phases.

NAC and bond length changes. NACs of chorismate are structures with a distance R between the two atoms C1 and C10 forming the new bond within the van der Waals contact distance of 3.7 Å and with the π-orbitals of atoms C1 and C10 pointing towards each other and allowing sufficient orbital overlap for the new bond formation. As a measure for the direction of the π-orbitals and their over-lap, Hur and Bruice [62] used the two angles ϕ_1 and ϕ_2, shown in Figure 1. They requested for a valid NAC that the deviations $\Delta\phi_1$ and $\Delta\phi_2$ from the ϕ_1 and ϕ_2 values of 8.2° and 18.6° obtained for **2** should be equal or smaller than ±20°. As shown in Figure 4(a), the C1C10 distances of reactions **R3**–**R6** meet the R criterion from the first point on the reaction path, **R1** and **R2** values are only slightly above. The data of Table 3 reveal that at M2, the beginning of the chemical phases, the NAC criteria are fulfilled by all reactions **R1**–**R6** including the gas phase, leading to the conclusion that on the basis of NACs the special enzyme activity cannot be explained.

Energy contribution of each reaction phase: Once the reaction phases are determined with URVA, the mechanistic details obtained from the curvature profiles can be complemented by the analysis of the energy contribution of each reaction phase to the reaction barrier, as shown in Figure 5, and Table 4 for reactions **R1**, **R3**, **R5**, and **R6**. All chemical events taking place before the TS cost energy, therefore this analysis provides a quick access to identifying these events and it can serve as a useful starting

Table 3. NAC parameters for reactions **R1**–**R6**, evaluated for the geometries at the reaction path curvature minima M2 and M3 (R in Ångstrom, ϕ_1 and ϕ_2 in degree).

	M2			M3		
Reaction	R(C1C10)	ϕ_1	ϕ_2	R	ϕ_1	ϕ_2
R1	3.41	23.9	32.7	2.84	5.5	24.6
R2	3.41	23.3	26.5	2.82	8.3	20.5
R3	3.15	17.0	21.8	2.76	8.6	17.1
R4	3.10	17.8	19.8	2.84	13.7	16.6
R5	3.10	17.8	19.4	2.82	8.4	16.8
R6	3.14	19.6	21.5	2.84	14.6	13.9
Definition [62]	≤ 3.7	8.2 ±20	18.6 ±20			

point for optimising and fine-tuning of a reaction. In the current study, we used this procedure to determine which phases of the rearrangement reaction are most energy consuming and how the energy consumption decreases from reaction **R1** to **R5** in order to deduce a rationale for the catalytic activity of the enzyme. There are two candidates: (i) the pre-chemical phases 1 and 2 and (ii) the chemical phases 3 and 4 up to the TS. As revealed by Figure 5 and the data in Table 4, the energy contribution of the pre-chemical phases 1 and 2 drops from 3.7 kcal/mol in **R1** to 0.1 kcal/mol in **R5**. So space confinement is only responsible for 26% of the 14 kcal/mol lowering of the energy barrier by the enzyme. The energy contribution of the chemical phase 3 drops from 15.6 kcal/mol in reaction **R1** to 7.2 kcal/mol in reaction **R5**, which corresponds to 60% of the barrier lowering, e.g. obviously the dominating enzyme function is to facilitate the CO bond breakage, which starts in reaction phase 3.

This observation can be further quantified by comparing the intrinsic strength of the CO bond to be broken for reactions **R1**–**R6**. The local mode force constants k^a and the related BSO n are the most qualified intrinsic bond strength measure, because they reflect all electronic effects influencing the strength of the bond

(a) **R1** gas phase

(b) **R3** water (TIP3P)

(c) **R5** BsCM(QM$_{ext}$/MM)

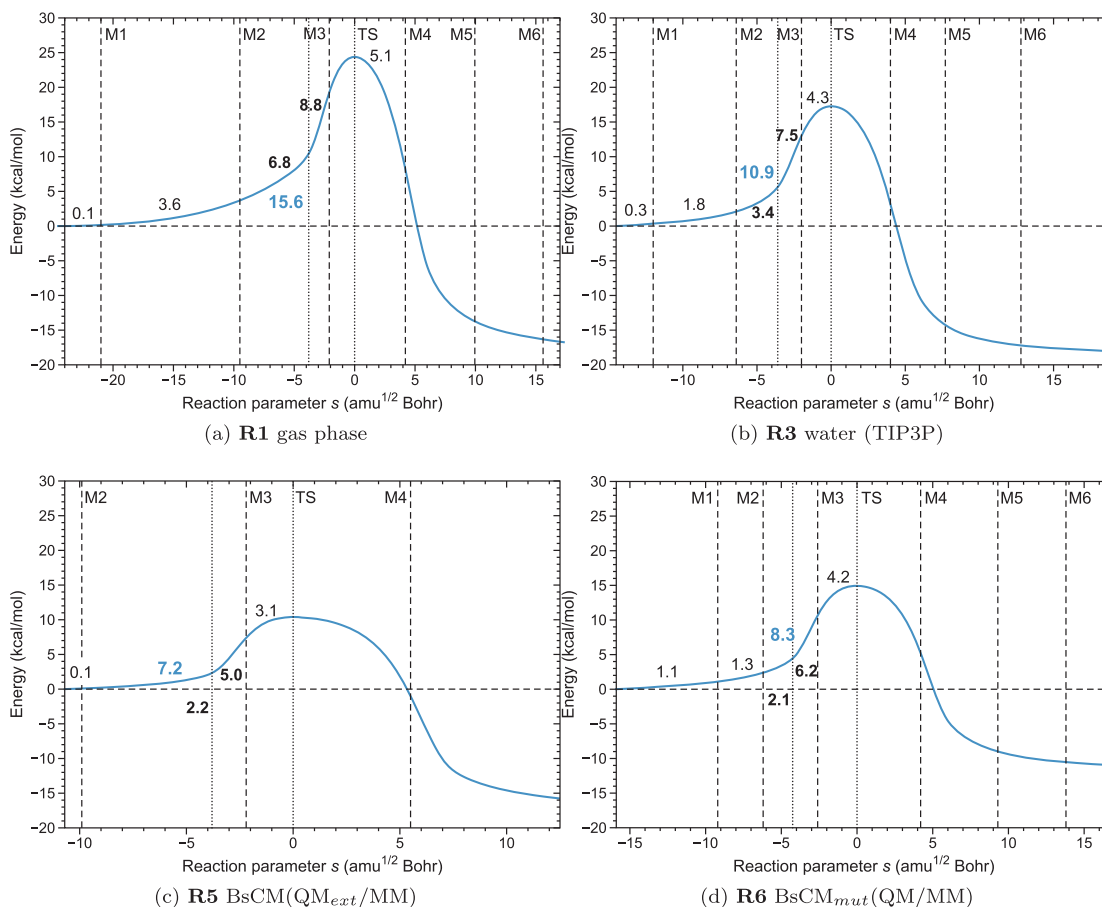(d) **R6** BsCM$_{mut}$(QM/MM)

Figure 5. Energy contribution of each reaction phase to the reaction barrier for reactions **R1**, **R3**, **R5**, and **R6**. The borders of the reaction phases are indicated by vertical dashed lines at curvature minima M1, M2, M3, etc. The position of the curvature maximum K1 and that of the TS at $s = 0$ amu$^{1/2}$ Bohr are also indicated by a vertical dotted line. The energy consumption in phase 3 (M2,M3) including the TS is split up into the contributions (M2,K1) and (K1,M3), both given in bold black print, the total contribution in phase 3 is also indicated.

Table 4. Energy contribution (En) of each reaction phase (Ph) to the reaction barrier for reactions **R1**, **R3**, **R5** and **R6**. Values in kcal/mol.

R1			R3			R5			R6		
Ph	En^a	En^b	Ph	En^a	En^b	Ph	En^a	En^b	Ph	En^a	En^b
1	0.1	0.1	1	0.3	0.3	1			1	1.1	1.1
2	3.6	3.7	2	1.8	2.1	2	0.1	0.1	2	1.3	2.4
3	15.6	19.3	3	10.9	13.0	3	7.2	7.3	3	8.3	10.7
4^c	5.1	24.4	4	4.3	17.3	4	3.1	10.4	4	4.2	14.9

^{a}Energy contribution of the reaction phase.
^{b}Energy at the end of the reaction phase.
^{c}Energy up to the TS contained in this phase.

under consideration including the effects form the environment, e.g. water or enzyme. The data in Table 5 and Figure 6 clearly reveal that the C6O8 bond strength of the reactant **1b** is directly related to the barrier height of the rearrangement reaction. We found the strongest C6O8 bond for the gas phase reaction **R1** with a CO bond length of 1.453 Å and a BSO of 0.797, a weakened C6O8 bond in aqueous solution, (R(C6O8) = 1.471 Å, BSO n = 0.736, reaction **R3**), and the weakest C6O8 bond for the enzyme

reaction **R5**, (R(C6O8) = 1.510 Å, BSO n = 0.609). It is interesting to note that the energy contribution to phase 3 (starting of the CO bond breakage) shows the same trend as revealed by Figure 6, e.g. already at the beginning of the rearrangement reaction the barrier height is already determined to a great extent. This is an important finding for catalyst optimisation and design. For a quick check, if a proposed modification moves into the right direction, e.g. weakening of the CO bond, it is not necessary to perform a whole new URVA study including the calculation of the reaction path. The Local Mode Analysis determining the CO bond strength just for the new reactant molecule is sufficient.

In summary, the analysis of the curvature profiles of **R1**–**R6** reveals in a comprehensive and elucidative way that the overall mechanism of bond breakage and bond formation is the same for gas phase, water, and enzyme environment, however that there are subtle differences in the pre- and post-chemical phases. Although space confinement plays a non-negligible role, a major contribution to the energy lowering by the enzyme results from
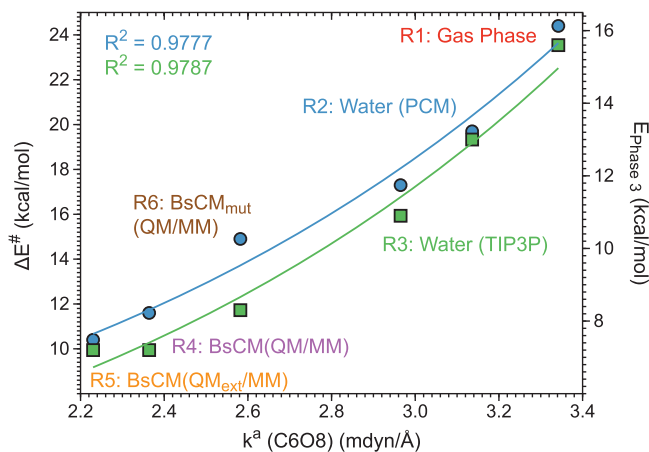
Figure 6. Correlation between the local force constant k^a(C6O8) of **1b** and the activation energy $\Delta E^{\ddagger}$ for reactions **R1–R6**, line and circles; correlation between the local force constant k^a(C6O8) of **1b** and the energy contribution E_{Phase3} to phase 3 for reactions **R1–R6**, line and squares.

Table 5. C6O8 and C1C10 distances R, local mode force constants k^a and BSO n for reactants **1b**, transition state **2(TS)**, and product **3** for reactions **R1–R6**.

Reaction	C6O8			C1C10		
	R (Å)	k^a (mDyn/Å)	BSO n^a	R (Å)	k^a (mDyn/Å)	BSO n^b
R1						
1b	1.453	3.342	0.797	3.786	–	–
2(TS)	2.138	0.140	0.096	2.672	–	–
3	3.845	–	–	1.542	3.713	0.930
R2						
1b	1.463	3.136	0.764	3.720	–	–
2(TS)	2.139	0.150	0.101	2.647	–	–
3	3.804	–	–	1.539	3.775	0.943
R3						
1b	1.471	2.965	0.736	3.366	0.122	0.060
2(TS)	2.108	0.280	0.153	2.586	0.218	0.096
3	3.510	0.035	0.038	1.584	2.780	0.738
R4						
1b	1.503	2.364	0.633	3.165	0.193	0.087
2(TS)	2.124	0.212	0.127	2.695	0.191	0.086
3	3.132	0.152	0.102	1.599	2.452	0.667
R5						
1b	1.510	2.230	0.609	3.112	0.201	0.090
2(TS)	2.122	0.196	0.120	2.694	0.198	0.089
3	3.157	0.144	0.098	1.592	2.543	0.687
R6						
1b	1.494	2.582	0.671	3.442	0.103	0.053
2(TS)	2.203	0.187	0.117	2.637	0.182	0.083
3	3.355	0.068	0.059	1.595	2.498	0.677

[a] References: CH_3OH and CH_2O, parameters $A = 0.35658, B = 0.66679$.
[b] References: C_2H_6, C_2H_4, parameters $A = 0.32519, B = 0.80129$, see text.

the alleviation of the CO bond cleavage, which is already determined when the active form **1b** docks into the active site of BsCM.

Decomposition of the path direction. In Figure 7, the decomposition of the reaction path direction into local components is shown for reactions **R1–R6**, which provides complementary information to the curvature analysis by disclosing the complexity of the reaction path. The path decomposition pattern is similar for all reactions and shows that the reaction is predominantly driven by the C6O8 and C1C10 parameters, which are closely coupled, typical of a pericyclic concerted reaction, in which one bond is broken and another bond is formed. First, the C1C10 takes the lead, then at curvature peak K1 C6O8 becomes dominant. At the curvature minimum M3, C6O8 adapts a maximal value and C1C10 a minimal value, both cross at K2 and then switch their roles. It is also obvious from Figure 5 that the reaction path is also determined to a signifiant extent by other internal coordinates. For example, the C9C10C1 and the C6O8C9 bond angles make a substantial contribution to the path direction. Therefore, earlier reaction path studies using a distinct reaction coordinate approach, which only considers the C6O8 and the C1C10 distance as path parameters can only be qualitative in nature [19, 53].

Ring puckering analysis. The Cremer–Pople puckering analysis [148–151] offers an important tool for the quantitative description of puckered rings and their conformational changes during a chemical reaction. According to Cremer and Pople, the puckering of a six-membered ring can be quantitatively described by the puckering amplitudes q_2 and q_3 and the pseudo-rotation phase angle ϕ_2, the hyperspherical angle Θ, and the total puckering amplitude Q. The pseudo-rotational coordinate pair (q_2, ϕ_2) describes the pseudo-rotation of boat and twist-boat forms of the six-membered ring, and the single crown puckering amplitude q_3 describes the chair. Based on these three coordinates the percentage of chair, boat, and twist-boat form can be determined (the corresponding formulas are provided in the online supplemental data).

The chorismate rearrangement is a challenging example, because it involves two six-membered rings, a cyclohexadienyl ring and an intermediate pyran ring. The puckering parameters of both rings for the stationary points **1b**, **2**, and **3** of reactions **R1–R6** are presented in Table 6. In addition, the percentage of the chair, boat and twist-boat conformation for each ring is given. Knowles and co-workers and others suggested that the rearrangement of **1b–3** proceeds through a transition state with a chair-like pyran ring [152–154]. This suggestion is quantified in this work by the results of our puckering analysis, presented in Table 6. The pyran ring of each TS of reactions **R1–R6** has a chair contribution between 81.9% (reaction **R6**) and 95.7% (reaction **R1**).

The conformation of the hexadienyl ring of all TSs (Table 6) is a mixture of chair and twist-boat for all reactions investigated in our study with the exception of the
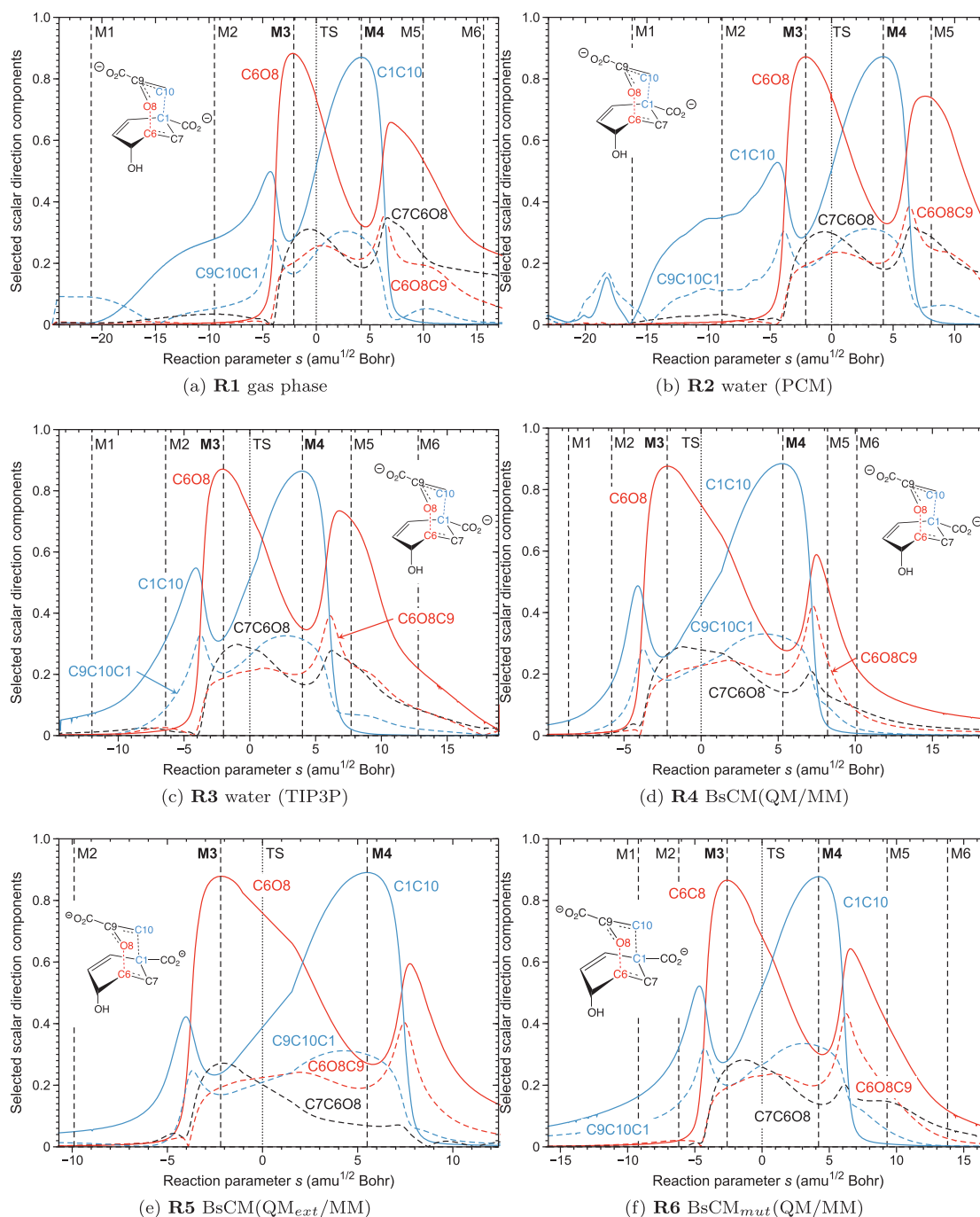
Figure 7. Decomposition of the reaction path direction into internal coordinate contribution for reactions **R1**–**R6**. (Only the most important contributions are shown.) The borders of the reaction phases are indicated by vertical dashed lines at curvature minima M1, M2, M3, etc. Curvature maxima are indicated by K1, K2, K3, etc. The TS at $s = 0$ amu$^{1/2}$ Bohr is indicated by a vertical dotted line.

TS of reaction **R4**, for which we found a boat conformation. However, including enzyme-chorismate H-bonding in reaction **R5**, the conformation of the hexadienyl ring of the TS has a similar mixture of the chair and twist-boat as found for the reactions in the gas phase and in aqueous solution. This reveals that the conformation of the hexadienyl ring of **2** reacts sensitively to the accurate description of the enzyme-substrate H-bonding. The hexadienyl

ring conformation of the **1b** molecules is a mixture of all three conformations, while that of **3** molecules is mainly dominated by the boat form allowing for the best placement of the two negatively charged carboxylate groups and their ϕ-delocalisation with the cycohexadienyl ring.

Electrostatic effects and H-bonding. In the following, we investigate the hypothesis that the catalytic function of BsCM is electrostatic TS stabilisation in combination

Table 6. Puckering parameters of the pyran ring and the cyclo-hexadienyl ring for reactions **R1**–**R6**.

Reaction	q_2 (Å)	q_3 (Å)	ϕ_2 (Deg)	Q (Å)	Chair (%)	Boat (%)	Tboat (%)
			Pyran Ring				
R1							
1b	0.16	−0.699	316	0.717	95	2.3	2.7
2(TS)	0.15	−0.713	296	0.729	95.7	4.1	0.2
3	0.285	−0.488	346	0.565	74.5	13.9	11.5
R2							
1b	0.279	−0.782	277	0.831	88.7	1.5	9.8
2(TS)	0.225	−0.73	285	0.763	91.3	4.5	4.1
3	0.171	−0.726	67	0.746	94.7	4.6	0.7
R3							
1b	0.379	−0.779	275	0.867	80.9	1.5	1.5
2(TS)	0.256	−0.724	283	0.768	88.9	4.6	6.5
3	0.114	−0.741	68	0.75	97.7	1.9	0.4
R4							
1b	0.306	−0.777	277	0.835	86.6	1.9	11.6
2(TS)	0.214	−0.752	286	0.782	92.5	3.9	3.6
3	0.144	−0.745	73	0.758	96.4	2.2	1.4
R5							
1b	0.285	−0.76	280	0.811	87.7	3.1	9.2
2(TS)	0.188	−0.737	290	0.761	93.9	4.7	1.4
3	0.162	−0.74	72	0.758	95.4	2.9	1.6
R6							
1b	0.451	−0.804	272	0.922	76.1	0.2	23.7
2(TS)	0.352	−0.749	279	0.827	81.9	3.7	14.3
3	0.074	−0.745	55	0.749	99	0.9	0.1
			Cyclohexadienyl Ring				
R1							
1b	0.226	0.092	168	0.244	14.2	56.7	29.1
2(TS)	0.123	0.091	96	0.153	35.5	6.4	58.1
3	0.349	0.013	182	0.350	0.1	98.3	1.6
R2							
1b	0.224	0.108	156	0.249	18.7	18.7	72.2
2(TS)	0.136	0.090	91	0.163	30.3	0.3	69.4
3	0.032	0.004	209	0.032	1.6	0.3	98.1
R3							
1b	0.224	0.126	138	0.257	23.8	27.0	49.1
2(TS)	0.142	0.095	88	0.171	30.9	1.0	68.1
3	0.255	0.004	358	0.256	0.0	99.3	0.7
R4							
1b	0.174	0.113	114	0.208	29.7	64.5	5.8
2(TS)	0.152	0.061	62	0.164	14	84.9	1.1
3	0.307	0.018	10	0.308	0.4	72.8	26.8
R5							
1b	0.202	0.131	134	0.241	29.6	37.5	32.9
2(TS)	0.119	0.081	94	0.143	31.6	3.5	64.9
3	0.251	0.021	5	0.252	0.7	92	7.3
R6							
1b	0.195	0.146	138	0.243	35.9	19.8	44.3
2(TS)	0.114	0.1	89	0.152	43.6	0.3	56.1
3	0.212	0.043	12	0.216	4.1	64.1	31.9

with enzyme-substrate H-bonding, as suggested by several authors [2, 33, 43, 56], and supported by biochemical data indicating that the positively charged Arg90 in BsCM stabilises the developing negative charge at the ether oxygen during the CO bond cleavage [19, 44, 48, 53]. This will also include a reexamination of the importance of the TS. Figure 8(a–d) features how the NBO charges on atoms O8, C6, C1, and C10 change during the chorismate rearrangement for reactions **R1**–**R6** from

the entrance to the exit channel. In the enzyme reaction **R5** starting at curvature peak K1 (beginning of CO breakage), the O8 atom picks up negative charge, reaching a maximum value of -680 me at curvature peak K2 (after the TS), and adapting its final value of −650 me at curvature peak K3 (finalization of CO bond breakage). This is a substantial amount compared for example with the charge transfer of about 18 me, which is sufficient in the Diels Alder reaction to start the pyramidalisation and subsequent bond equalisation of the ethylene and butadiene units [73]. In the case of the modified enzyme reaction **R6**, the pick up of negative charge is less pronounced, revealing the importance of the positive charge of the vicinal Arg90, which makes the CO bond cleavage more heterolytic in the enzyme environment.

The changes of the charge of bond partner C6 are more uniform along *s*, as shown in Figure 8(b). In all media, C6 starts with a small, positive charge. At curvature peak K1, C6 starts to pick up a negative charge, reflecting its change from an sp^3 hybridised carbon atom with a formal σ bond with O8 to an sp^2 hybridised carbon atom with a σ and a π bond to carbon. Interestingly, the increased heterolytic character of the C6O8 cleavage in the enzyme is not transferred to a similarly increased heterolytic C1C10 bond formation. In all media, C1 starts with a negative charge of about 150 me, which remains fairly constant until curvature peak K1, see Figure 8(c). After passing through a minimum value of 3 me at curvature peak K2, C1 picks up a negative charge until adapting its final value of about −250 me around curvature peak K3 (finalization of CC bond formation). C10 is negatively charged in the entrance channel spanning a range of −440 me in the enzyme to −520 me in the gas phase, see see Figure 8(d). This is reflecting that in the entrance channel C10 is more exposed to the environment. Like C6, it picks up a negative charge until reaching at K3 a final value of about −550 me. This leads to the conclusion that the acceleration of CO bond cleavage has an external reason caused by charges in the immediate environment rather than introduced by intermolecular interactions. Water molecules with their H-bonding facilities can assist the CO bond cleavage only to a certain extent as their H-bonding capabilities involve more the carboxylate groups, and therefore have only an indirect effect on the cleavage of C6O8 [155–159], which means that only a moderate lowering of the energy barrier can be expected, in line with the observations made in this work.

It has been speculated that the charge polarisation caused by the intermolecular hydrogen bonds with the enzyme leads in turn to an intramolecular charge transfer or electron polarisation from the enolpyruvyl part to the cylohexadienyl unit. Decreasing in this way the
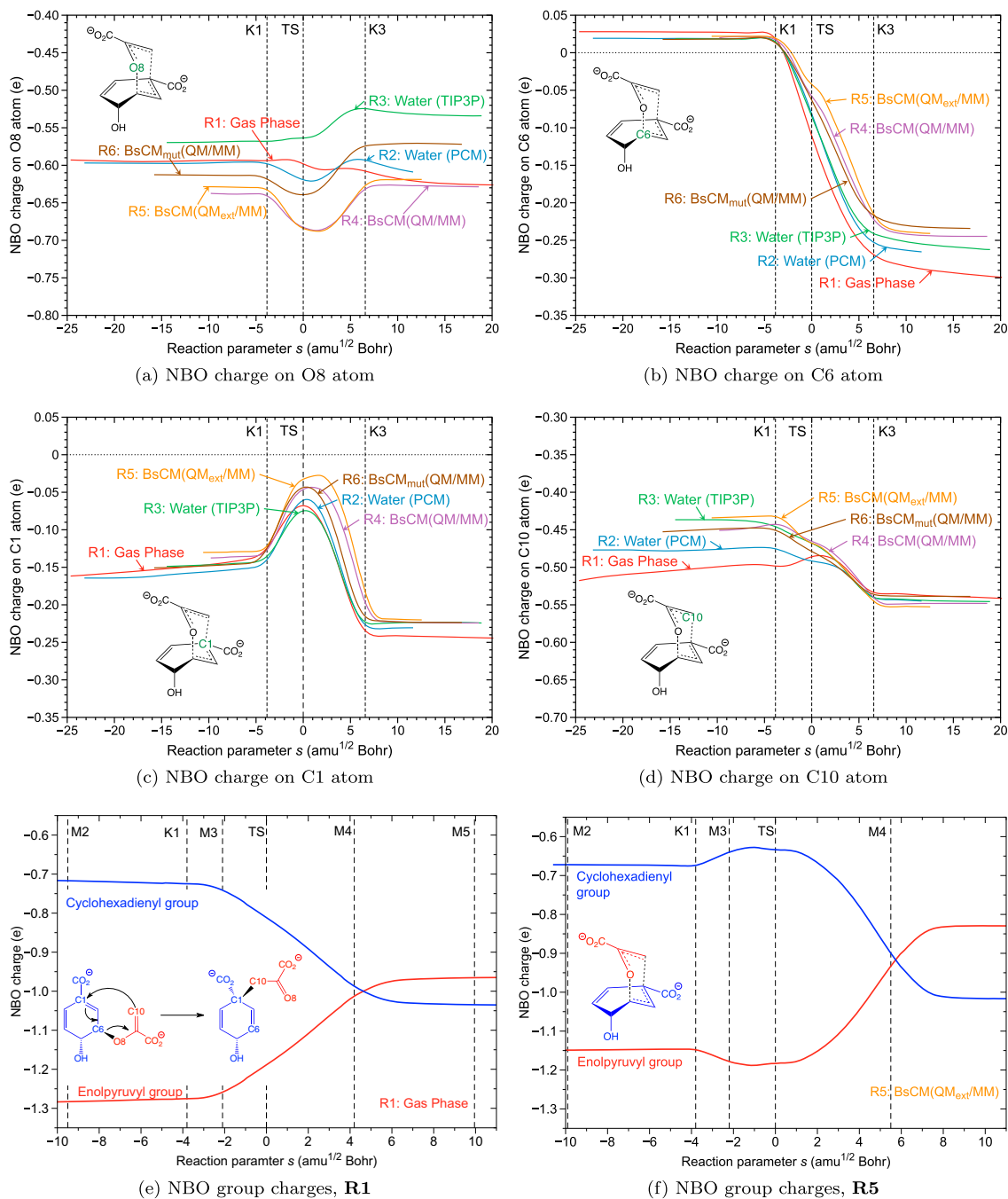
Figure 8. (a)–(d): NBO charges on atoms O8, C6 C1 and C10 as a function of the reaction parameter s for the reactions **R1**–**R6**. (e,f): NBO charge of the enolpyruvyl group and the NBO charge of the 4-hydroxy-1,5-cyclohexdiene-1-carboxylate group as function of the reaction parameter s for the reactions **R1** and **R5**. The TS at $s = 0$ amu$^{1/2}$ Bohr is indicated by a vertical dashed line.

repulsion between the two negatively charged carboxylate groups, which have to come closer to form **3**, should lead to an acceleration of the rearrangement [33]. Figure 8(e,f) present the total NBO charge of the enolpyruvyl group and that of the 4-hydroxy-1,5-cyclohexdiene-1-carboxylate group as function of the reaction parameter s for the reactions **R1** and **R5**, respectively. In the gas phase, the enolpyruvyl group starts

with a negative charge of -1290 me, the cyclohexadienly group with a negative charge of -715 me, at K1 charge transfer from enolpyruvyl to cyclohexadienly starts until at curvature minimum M4 both parts are equally charged, after that a small charge transfer occurs in the opposite direction leading to a final charge of the enolpyruvyl group of -967 me and that of the hexadienyl group of -1036 me, see Figure 8(e). It is interesting

to note that in the enzyme reaction **R5** the charge difference between the two part is smaller from the beginning, goes through a maximum around the TS, becomes again zero at M4 as in the case of **R1**, and then the charge transfer occurs again in the opposite direction until the final values of −830 me for the enolpyruvyl and −1016 me for the cyclohexdienyl group are reaching at 7.5 s units, see 8(f). The remaining charge of −154 me is transferred to the enzyme. This analysis shows that the charge transfer in the enzyme from the enolpyruvyl to the cyclohexdienyl group occurs after the TS and, therefore cannot contribute to the lowering of the energy barrier.

Several authors emphasised that the BsCM lowers the barrier by selective H-bonding with the TS [18, 43, 48, 52, 155, 156]. Most of these studies discuss enzyme-TS H-bonding based on geometric features, e.g. H-bond distances leading to an overview of the H-bond network. However, H-bond distances do not necessarily provide a measure of the bond strength. The shorter bond is not always the stronger bond [107, 108, 160]. In this work, enzyme-substrate H-bonding was quantitatively assessed for the first time with the Local Mode Analysis, which provides the intrinsic strength of a hydrogen bond on the basis of the local H-bond force constant and related BSO [101–103, 113].
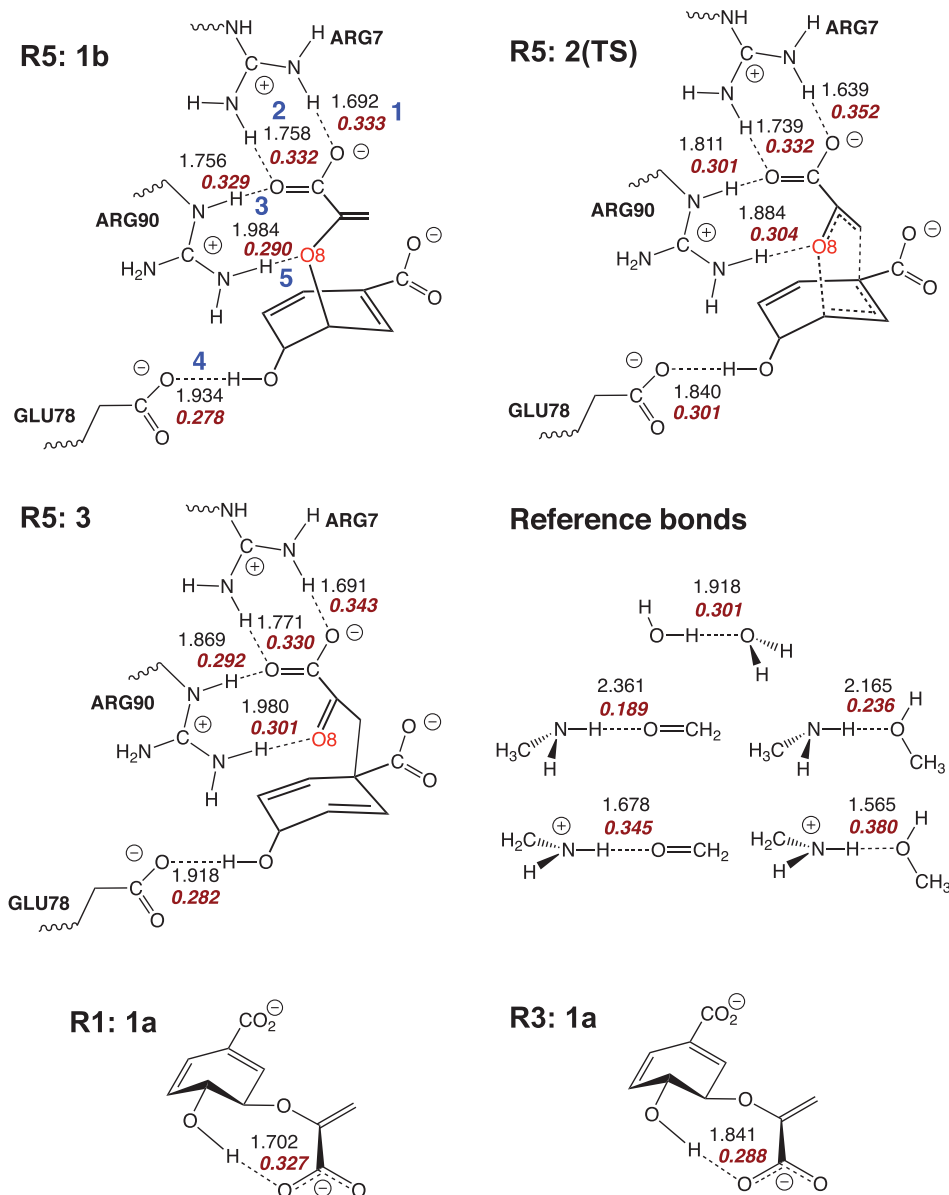

Figure 9. H-bond distances(in Ångstrom, regular print) and BSO *n* values (italics print) for the intermolecular hydrogen bonds in **1b**, **2(TS)**, and **3** of reaction **R5** and some reference molecules, and for the intramolecular H-bonds in **1a** for reactions **R1** and **R3**. The five H-bonds in the enzyme are numbered - in order to facilitate the discussion.

In Figure 9, the intermolecular H-bonds between BsCM and **1b**, **2(TS)**, and **3** of reaction **R5** are shown, revealing that the H-bond network between the enzyme and the substrate does not change during the rearrangement, e.g. the enzyme confines the RC in an optimal position for the rearrangement from the very start of the reaction. This is fully in line with our finding that in the enzyme there is no longer a pre-chemical phase needed to rearrange the reacting parts of the chorismate. The carboxylate group of the enolpyruvyl part of the reactant **1b** forms two strong H-bonds with Arg7 (BSO values: of 0.332 and 0.333 for H-bonds 1 and 2, respectively) and one H-bond with Arg90 (BSO value of 0.329 for H-bond 3). While the inner H-bond 2 does not change its intrinsic strength in TS **2**, H-bond 3 becomes marginally weaker (BSO value of 0.301 vs 0.329) and H-bond 1 marginally stronger (BSO value of 0.352 vs. 0.333). In the product **3**, H-bonds 1 an 3 becomes marginally weaker compared to TS **2**. The cylohexadienyl group is fixed via H-bond 4 between the hydroxyl substituent and Glu78 (BSO values of 0.278, 0.301, and 0.282 for **1b**, TS **2**, and **3**, respectively), showing a slightly stronger H-bond for the TS. Most interesting is the H-bond 5 between the ether oxygen O8 and Arg90, which has been targeted in several studies as the major source for the enzyme-TSstabilisation [18, 43, 48, 52, 155, 156]. This is not confirmed by the Local Mode Analysis. We found only a slight increase of the BSO value for H-bond 5 for TS **2** (BSO value of 0.304 compared with 0.290 for **1b** and 0.301 for **3**), again confirming that overall there is nothing special about the TS.

In Figure 9 (bottom), the intermolecular H-bonds are shown for **1a** in the gas phase **R1** and in aqueous solution **R3**. The H-bond in gas phase is considerably stronger than the H-bond in the water dimer (BSO value of 0.327 compared to 0.301) explaining the conversion barrier of 12.2 kcal/mol for the diequatorial-diaxial conversion **1a** → **1b**, which is primarily caused by the cleavage of this H-bond (see the corresponding energy and curvature profiles of **1a** → **1b** in the online supplemental data). In aqueous solution, the intermolecular H-bond is weakened because both the hydroxyl substituent of the cyclohexadienyl group and the carboxylate of the enolpyruvyl group can engage in H-bonding with the surrounding water molecules. This is reflected by a decreased BSO value of 0.288, in line with the substantial lower conversion barrier of 4.8 kcal/mol and a much smaller energy difference between **1a** and **1b** of 3.7 kcal/mol compared with the gas phase difference of 11.9 kcal/mol.

Gold catalysis of the chorismate rearrangement. This section is devoted to a comparison of what Nature does to lower the barrier of the chorismate rearrangement with homogenous transition metal catalysis. Guided by our recent study of the Gold(I)-assisted [3,3]-sigmatropic rearrangement of allyl acetate [70], we investigated the chorismate rearrangement of **1b** to **3** in the gas phase with a AuCl catalyst attached, reaction **R7** as shown in Figure 1. Au(I) species are soft Lewis acids with high carbophilic character and a high affinity to coordinate with π-systems [161, 162]. Like in the case of the Gold(I)-assisted [3,3]-sigmatropic rearrangement of allyl acetate, the Au(I) catalyst breaks up the reactions into two steps by acting as a *chameleon*, e.g. easily switching between Au[I]-π and Au[I]-σ complexation.

(a) Step 1 of reaction **R7**
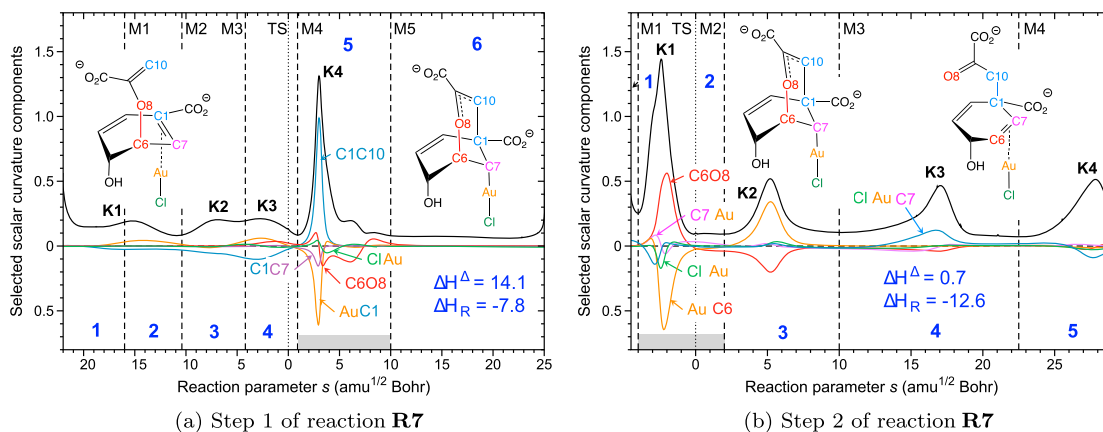
(b) Step 2 of reaction **R7**

Figure 10. Scalar curvature as a function of the reaction path parameter s (solid black line) for the AuCl catalysed chorismate rearrangement **R7** in the gas phase. The decomposition of the scalar curvature into components is given. The borders of the reaction phases are indicated by vertical dashed lines at curvature points M1, M2, M3, etc. Curvature maxima are indicated by K1, K2, K3, etc. The TS at $s = 0$ amu$^{1/2}$ Bohr is also indicated by a vertical dashed line. The reaction phases are denoted in blue print and the chemical phases are highlighted with a grey bar.

Figure 10 shows the curvature profile for both reaction steps. The first step (see Figure 10(a)) follows a six-phase mechanism. The pre-chemical phases 1–4, including the TS stretch over more than 20 s units. There are only small curvature enhancements, which result from the rotation of the enolpyruvyl side chain bringing the atoms C1 and C10 closer together. Simultaneously, the AuCl part moves towards atom C7 in order to transform from a Au[I]-π and Au[I]-σ complex (see video in the online supplemental data). This is an energy saving, exothermic process reflected by an activation enthalpy $\Delta H^{\ddagger}$ of 14.1 kcal/mol and reaction enthalpy ΔH_R of -7.8 kcal/mol. Important to note is (i) that the chemical phase between M4 and M5 occurs after the TS, e.g. the formation of the new C1C10 bond and formation of the Au[I]-σ complex does not require additional energy; (ii) that in contrast to reactions **R1**–**R6**, the CO bond is not broken, it stays intact. This is a drastic change of the chemical mechanism, moving the energy demanding CO cleavage out of the first reaction step. In the second step, see Figure 10(b), which has an activation enthalpy $\Delta H^{\ddagger}$ of only 0.72 kcal/mol, the Au[I]-σ transforms back into a more stable Au[I]-π complex ($\Delta H_R = -12.6$ kcal/mol), supporting CO bond cleavage, which stretches over phases 3–6. As shown in the corresponding video (see online supplemental data), the carboxylate anion group attached to C1 rotates like a screwdriver pushing the C6 and O8 atoms apart.

4. Conclusions and outlook

In this work, we investigated the mechanism of the chorismate rearrangement in the gas phase, in solution and catalysed by BsCM using the URVA analysis as a powerful mechanistic tool, that allows a one-to-one comparison of a chemical reaction in different environments. In combination with the Local Mode Analysis some current assumptions about the enzyme catalysed chorismate rearrangement could be confirmed and quantified, others refuted, and new valuable aspects shedding new light into the enzyme activity were derived, which led to the following conclusions:

- The analysis of the reaction path curvature indisputably confirmed that the actual mechanism of the chorismate rearrangement is the same in the gas phase, solution and enzyme. The process of CO bond cleavage starts before the TS and the new CC bond formation is finalised after the TS. There are subtle differences in the pre-chemical phases, which are a result of the different environments. The pre-chemical phases become shorter in aqueous solution and disappear for the enzyme reaction, i.e. the chemical process of CO bond cleavage starts right away.

- These findings were corroborated by the analysis of the H-bond network between the enzyme and reactant, TS, and product, respectively, revealing that the H-bond network does not change during the rearrangement, e.g. the enzyme confines the reaction complex in an optimal position for the rearrangement from the very start of the reaction. This also holds for the intrinsic strength of these H-bonds, measured via the local H-bond force constants, which stays fairly constant during the reaction. In particular, the intrinsic strength of the H-bond between the ether oxygen O8 and Arg90 increases only marginally from the reactant to the TS, thus refuting suggestions that this H-bond is the major source for enzyme-TS stabilisation leading to a lower barrier.

- Although being an integral part of the enzyme catalysis, space confinement does not play the leading role for the lowering of the reaction barrier. The major effect of the enzyme is that of an electrostatic embedment of the reaction complex, which shifts the CO bond cleavage from a more homolytic to a more heterolytic type, due to the positioning of the charged Arg90 in a well-defined vicinity to the reaction complex. The intrinsic strength of the CO bond to be broken predominantly determines the barrier height. The CO bond is weakest in the enzyme environment in accordance with the lowest barrier found for the enzyme reaction. Interesting to note is that this is already reflected by the intrinsic CO bond strength of the reactant, e.g. the fate of the reaction is already determined early in the entrance channel. This is an important finding for catalyst optimisation and design. For a quick check if a proposed modification moves into the right direction, i.e. weakening of the CO bond, it is not necessary to perform a whole new URVA study. A Local Mode Analysis determining the CO bond strength for the new reactant molecule is sufficient.

- In contrast to the enzyme reaction, the gas phase rearrangement catalysed by AuCl shows a drastically changed chemical mechanism. The reaction is split into two steps by switching between Au[I]-π and Au[I]-σ complexation. In the first step, the new CC bond is formed. The energy consuming CO bond cleavage is moved into the second step, where it is facilitated by the back-switch of the intermediate Au[I]-σ to the final Au[I]-π complex.

Inspired by the results of this study, we are in the process of combining the two different strategies, CO bond weakening as supported by the enzyme and splitting the rearrangement into two parts as performed by the gold(I) catalyst.

Acknowledgments

Disclosure statement

No potential conflict of interest was reported by the authors.

Funding

ORCID

Marek Freindorf http://orcid.org/0000-0001-5285-5455
Daniel Sethio http://orcid.org/0000-0002-8075-1482
Elfi Kraka http://orcid.org/0000-0002-9658-5626

References

[1] C.T. Walsh and Y. Tang, Biochemistry **57** (22), 3087–3104 (2018).
[2] A.L. Lamb, Biochemistry **50** (35), 7476–7483 (2011).
[3] E. Haslam, *Shikimic Acid: Metabolism and Metabolites* (John Wiley & Sons, New York, 1993).
[4] R. Mir, S. Jallu and T.P. Singh, Crit. Rev. Microbiol. **41** (2), 172–189 (2013).
[5] H. Maeda and N. Dudareva, Annu. Rev. Plant Biol. **63** (1), 73–105 (2012).
[6] A.R. Nazmi, E.J.M. Lang, Y. Bai, T.M. Allison, M.H. Othman, S. Panjikar, V.L. Arcus and E.J. Parker, J. Biol. Chem. **291** (42), 21836–21847 (2016).
[7] J. Pittard and F. Gibson, Curr. Top. Cell. Reg. **2**, 29–63 (2016).
[8] D.J. Cole and N.D.M. Hine, J. Phys. Condens. Matter **28** (39), 393001–3930030 (2016).
[9] C.L. Ramírez, M.A. Martí and A.E. Roitberg, Chapter Six - Steered Molecular Dynamics Methods Applied to Enzyme Mechanism and Energetics. Vol. 578, 1st ed. (Elsevier Inc., Amsterdam, 2016), pp. 123–143.
[10] G. Jindal and A. Warshel, J. Phys. Chem. B **120** (37), 9913–9921 (2016).
[11] P. Sokkar, E. Boulanger, W. Thiel and E. Sanchez-Garcia, J. Chem. Theory Comput. **11** (4), 1809–1818 (2015).
[12] M. Sanchez-Martinez, M. Field and R. Crehuet, J. Phys. Chem. B **119** (3), 1103–1113 (2014).
[13] G.J. Cheng, X. Zhang, L.W. Chung, L. Xu and Y.D. Wu, J. Am. Chem. Soc. **137** (5), 1706–1725 (2015).
[14] G. Lever, D.J. Cole, R. Lonsdale, K.E. Ranaghan, D.J. Wales, A.J. Mulholland, C.K. Skylaris and M.C. Payne, J. Phys. Chem. Lett. **5** (21), 3614–3619 (2014).
[15] N. Lawan, K.E. Ranaghan, F.R. Manby and A.J. Mulholland, Chem. Phys. Lett. **608**, 380–385 (2014).
[16] M.W. Van Der Kamp and A.J. MulhollandBiochemistry **52** (16), 2708–2728 (2013).
[17] K. Meier, A. Choutko, J. Dolenc, A.P. Eichenberger, S. Riniker and W.F. Van Gunsteren, Angew. Chemie – Int. Ed. **52** (10), 2820–2834 (2013).
[18] T. Ishida, J. Am. Chem. Soc. **132** (20), 7104–7118 (2010).
[19] T. Ishida, D.G. Fedorov and K. Kitaura, J. Phys. Chem. B **110** (3), 1457–1463 (2006).
[20] H. Guo and N. Rao, in *Claisen Rearrange. Appl.*, edited by U. Hiersemann, M. Nubbemeyer and Chap. Chorismate (John Wiley & Sons, Ltd., New York, 2007), pp. 571–594.
[21] F. Claeyssens, J.N. Harvey, F.R. Manby, R.A. Mata, A.J. Mulholland, K.E. Ranaghan, M. Schütz, S. Thiel, W. Thiel and H.J. Werner, Angew. Chemie Int. Ed. **45** (41), 6856–6859 (2006).
[22] A. Crespo, M.A. Martí, D.A. Estrin and A.E. Roitberg, J. Am. Chem. Soc. **127** (19), 6940–6941 (2005).
[23] K.E. Ranaghan, L. Ridder, B. Szefczyk, W.A. Sokalski, J.C. Hermann and A.J. Mulholland, Org. Biomol. Chem. **2** (7), 968–980 (2004).
[24] K.E. Ranaghan, L. Ridder, B. Szefczyk, W.A. Sokalski, J.C. Hermann and A.J. Mulholland, Mol. Phys. **101**, 2695–2714 (2009).
[25] S.E. Worthington, A.E. Roitberg and M. Krauss, J. Phys. Chem. B **105** (29), 7087–7095 (2001).
[26] P.D. Lyne, A.J. Mulholland and W.G. Richards, J. Am. Chem. Soc. **117** (45), 11345–11350 (1995).
[27] G. Jindal and A. Warshel, Proteins: Struct. Funct. Bioinf. **85** (12), 2157–2161 (2017).
[28] S.R. Pruitt and C. Steinmann, J. Phys. Chem. A **121** (8), 1797–1807 (2017).
[29] M. Karelina and H.J. Kulik, J. Chem. Theory Comput. **13** (2), 563–576 (2017).
[30] T. Benighaus and W. Thiel, J. Chem. Theory Comput. **7** (1), 238–249 (2011).
[31] H.M. Senn and W. Thiel, Angew. Chem. Int. Ed. **48** (7), 1198–1229 (2009).
[32] H.M. Senn, J. Kästner, J. Breidung and W. Thiel, Can. J. Chem. **87** (10), 1322–1337 (2009).
[33] F. Claeyssens, K.E. Ranaghan, N. Lawan, S.J. Macrae, F.R. Manby, J.N. Harvey and A.J. Mulholland, Org. Biomol. Chem. **9** (5), 1578–1590 (2011).
[34] Q. Cui, J. Chem. Phys. **145** (14), 140901–140913 (2016).
[35] S.S. Patel, Ph. D. thesis, Massachusetts Institute of Technology, Department of Chemistry, 2015.
[36] P.R. Andrews, G.D. Smith and I.G. Young, Biochemistry **12** (18), 3492–3498 (1973).
[37] P.A. Bartlett, Y. Nakagawa, C.R. Johnson, S.H. Reich and A. Luis, J. Org. Chem. **53** (14), 3195–3210 (1988).
[38] Y.M. Chook, H. Ke and W.N. Lipscomb, Proc. Natl. Acad. Sci. **90** (18), 8600–8603 (1993).
[39] Y.M. Chook, J.V. Gray, H. Ke and W.N. Lipscomb, J. Mol. Biol. **240** (5), 476–500 (1994).
[40] P. Kast, C. Grisostomi, I.A. Chen, S. Li, U. Krengel, Y. Xue and D. Hilvert, J. Biol. Chem. **275** (47), 36832–36838 (2000).
[41] A. Choutko, A.P. Eichenberger, W.F. van Gunsteren and J. Dolenc, Protein Sci. **22** (6), 809–822 (2013).
[42] J.E. Culbertson, D.H. Chung, K.T. Ziebart, E. Espiritu and M.D. Toney, Biochemistry **54** (14), 2372–2384 (2015).
[43] D. Burschowsky, U. Krengel, E. Uggerud and D. Balcells, FEBS Open Bio **7** (6), 789–797 (2017).
[44] D. Burschowsky, A. van Eerde, M. Okvist, A. Kienhöfer, P. Kast, D. Hilvert and U. Krengel, Proc. Natl. Acad. Sci. USA **111**, 17516–17521 (2014).
[45] D.W. Gohara and E. Di Cera, J. Biol. Chem. **291** (40), 20840–20848 (2016).
[46] M.M. Davidson, I.R. Gould and I.H. Hillier, J. Chem. Soc., Perkin Trans. 2 **1** (4), 525–531 (1996).

[47] S.T. Cload, D.R. Liu, R.M. Pastor and P.G. Schultz, J. Am. Chem. Soc. **118** (7), 1787–1788 (1996).

[48] A. Kienhöfer, P. Kast and D. Hilvert, J. Am. Chem. Soc. **125** (11), 3206–3207 (2003).

[49] P. Kast, M. Asif-Ullah, N. Jiang and D. Hilvert, Proc. Natl. Acad. Sci. **93** (10), 5043–5048 (1996).

[50] P. Kast, Y.B. Tewari, O. Wiest, D. Hilvert, K.N. Houk and R.N. Goldberg, J. Phys. Chem. B **101** (50), 10976–10982 (1997).

[51] N.A. Khanjin, J.P. Snyder and F.M. Menger, J. Am. Chem. Soc. **121** (50), 11831–11846 (1999).

[52] H. Guo, Q. Cui, W.N. Lipscomb and M. Karplus, Angew. Chemie – Int. Ed. **42** (13), 1508–1511 (2003).

[53] C.R.W. Guimaräes, M. Udier-Blagović, I. Tubert-Brohman and W.L. Jorgensen, J. Chem. Theory Comput. **1** (4), 617–625 (2005).

[54] L. Dong and Y. Liu, Proteins: Struct. Funct. Bioinform. **85** (6), 1146–1158 (2017).

[55] S. Martí, J. Andrés, V. Moliner, E. Silla, I. Tuñón and J. Bertrán, Theor Chem. Acc. **105** (3), 207–212 (2001).

[56] M. Štrajbl, A. Shurki, M. Kato and A. Warshel, J. Am. Chem. Soc. **125** (34), 10228–10237 (2003).

[57] V.L. Arcus, E.J. Prentice, J.K. Hobbs, A.J. Mulholland, M.W. Van der Kamp, C.R. Pudney, E.J. Parker and L.A. Schipper, Biochemistry **55** (12), 1681–1688 (2016).

[58] L. Pauling, Chem. Eng. News **24**, 1375–1377 (1946).

[59] S.K. Sadiq and P.V. Coveney, J. Chem. Theory Comput. **11** (1), 316–324 (2014).

[60] J. Zhang, Y.I. Yang, L. Yang and Y.Q. Gao, J. Phys. Chem. B **119** (17), 5518–5530 (2015).

[61] S. Hur and T.C. Bruice, Proc. Natl. Acad. Sci. **99** (3), 1176–1181 (2002).

[62] S. Hur and T.C. Bruice, Proc. Natl. Acad. Sci. U. S. A. **100** (21), 12015–12020 (2011).

[63] S. Hur and T.C. Bruice, J. Am. Soc. Chem. **125** (6), 1472–1473 (2003).

[64] X. Zhang, X. Zhang and T.C. Bruice, Biochemistry **44**, 10443–10448 (2005).

[65] M. Štrajbl, A. Shurki, M. Kato and A. Warshel, J. Am. Chem. Soc. **125** (34), 10228–10237 (2003).

[66] M. Garcia-Viloca, J. Gao, M. Karplus and D.G. Truhlar, Science **303** (5655), 186–195 (2004).

[67] S.J. Benkovic, G.G. Hammes and S. Hammes-Schiffer, Biochemistry **47** (11), 3317–3321 (2008).

[68] A. Warshel and R.P. Bora, J. Chem. Phys. **144** (18), 180901–180918 (2016).

[69] P. Kast, M. Asif-Ullah and D. Hilvert, Tetrahedron Lett. **37** (16), 2691–2694 (1996).

[70] M. Freindorf, D. Cremer and E. Kraka, Mol. Phys. **116** (5-6), 611–630 (2017).

[71] M.C. Reis, C.S. López, E. Kraka, D. Cremer and O.N. Faza, Inorg. Chem. **55** (17), 8636–8645 (2016).

[72] C.S. López, O.N. Faza, M. Freindorf, E. Kraka and D. Cremer, J. Org. Chem. **81** (2), 404–414 (2015).

[73] T. Sexton, E. Kraka and D. Cremer, J. Phys. Chem. A **120** (7), 1097–1111 (2016).

[74] M. Freindorf, T. Sexton, E. Kraka and D. Cremer, Theor. Chem. Acc. **133** (1), 1423–1441 (2014).

[75] E. Kraka, W. Zou, M. Freindorf and D. Cremer, J. Chem. Theory Comput. **8** (12), 4931–4943 (2012).

[76] E. Kraka, H. Joo and D. Cremer, Mol. Phys. **108** (19–20), 2667–2685 (2010).

[77] W. Zou, T. Sexton, E. Kraka, M. Freindorf and D. Cremer, J. Chem. Theory Comput. **12** (2), 650–663 (2016).

[78] E. Kraka, WIREs: Comput. Mol. Sci. **1** (4), 531–556 (2011).

[79] Z. Konkoli and D. Cremer, Int. J. Quant. Chem. **67** (1), 1–9 (1998).

[80] Z. Konkoli, J.A. Larsson and D. Cremer, Int. J. Quant. Chem. **67** (1), 11–27 (1998).

[81] Z. Konkoli and D. Cremer, Int. J. Quant. Chem. **67** (1), 29–40 (1998).

[82] Z. Konkoli, J.A. Larsson and D. Cremer, Int. J. Quant. Chem. **67** (1), 41–55 (1998).

[83] W. Zou, R. Kalescky, E. Kraka and D. Cremer, J. Chem. Phys. **137** (8), 084114 (2012).

[84] W. Zou and D. Cremer, Theor. Chem. Acc. **133**, 1451–1466 (2014).

[85] W.H. Miller, N.C. Handy and J.E. Adams, J. Chem. Phys. **72** (1), 99–112 (1980).

[86] E. Kraka and D. Cremer, Acc. Chem. Res. **43** (5), 591–601 (2010).

[87] D. Cremer and E. Kraka, Curr. Org. Chem. **14**, 1524–1560 (2010).

[88] D. Cremer and J.A. Pople, J. Am. Chem. Soc. **97**, 1354–1358 (1975).

[89] T.M. Sexton, M. Freindorf, E. Kraka and D. Cremer, J. Phys. Chem. A **120** (42), 8400–8418 (2016).

[90] E.B. Wilson, J.C. Decius and P.C. Cross, *Molecular Vibrations. The Theory of Infrared and Raman Vibrational Spectra* (McGraw-Hill, New York, 1955).

[91] W. Zou and D. Cremer, Chem. Eur. J. **22**, 4087–4099 (2016).

[92] D. Cremer, J.A. Larsson and E. Kraka, in *Theoretical and Computational Chemistry*, edited by C. Parkanyi (Elsevier, Amsterdam, 1998), pp. 259–327.

[93] J. Oomens, E. Kraka, M.K. Nguyen and T.M. Morton, J. Phys. Chem. A **112** (43), 10774–10783 (2008).

[94] W. Zou, R. Kalescky, E. Kraka and D. Cremer, J. Mol. Model. **19** (7), 2865–2877 (2013).

[95] R. Kalescky, E. Kraka and D. Cremer, J. Phys. Chem. A **117** (36), 8981–8995 (2013).

[96] R. Kalescky, E. Kraka and D. Cremer, J. Phys. Chem. A **118** (1), 223–237 (2014).

[97] R. Kalescky, E. Kraka and D. Cremer, Inorg. Chem. **53** (1), 478–495 (2013).

[98] R. Kalescky, E. Kraka and D. Cremer, Int. J. Quant. Chem. **114** (16), 1060–1072 (2014).

[99] R. Kalescky, W. Zou, E. Kraka and D. Cremer, J. Phys. Chem. A **118** (10), 1948–1963 (2014).

[100] A. Humason, W. Zou and D. Cremer, J. Phys. Chem. A. **119** (9), 1666–1682 (2014).

[101] M. Freindorf, E. Kraka and D. Cremer, Int. J. Quant. Chem. **112** (19), 3174–3187 (2012).

[102] R. Kalescky, W. Zou, E. Kraka and D. Cremer, Chem. Phys. Lett. **554**, 243–247 (2012).

[103] R. Kalescky, E. Kraka and D. Cremer, Mol. Phys. **111** (9–11), 1497–1510 (2013).

[104] E. Kraka, M. Freindorf and D. Cremer, Chirality **25** (3), 185–196 (2013).

[105] D. Setiawan, E. Kraka and D. Cremer, Chem. Phys. Lett. **614**, 136–142 (2014).

[106] D. Setiawan, E. Kraka and D. Cremer, J. Phys. Chem. A **119** (9), 1642–1656 (2014).

[107] D. Setiawan, E. Kraka and D. Cremer, J. Phys. Chem. A **119** (36), 9541–9556 (2015).

[108] E. Kraka, D. Setiawan and D. Cremer, J. Comp. Chem. **37** (1), 130–142 (2015).

[109] X. Zhang, H. Dai, H. Yan, W. Zou and D. Cremer, J. Am. Chem. Soc. **138** (13), 4334–4337 (2016).

[110] D. Setiawan and D. Cremer, Chem. Phys. Lett. **662**, 182–187 (2016).

[111] V. Oliveira, E. Kraka and D. Cremer, Phys. Chem. Chem. Phys. **18** (48), 33031–33046 (2016).

[112] V. Oliveira, E. Kraka and D. Cremer, Inorg. Chem. **56** (1), 488–502 (2016).

[113] Y. Tao, W. Zou, J. Jia, W. Li and D. Cremer, J. Chem. Theory Comput. **13** (1), 55–76 (2016).

[114] V. Oliveira and D. Cremer, Chem. Phys. Lett. **681**, 56–63 (2017).

[115] V. Oliveira, D. Cremer and E. Kraka, J. Phys. Chem. A **121** (36), 6845–6862 (2017).

[116] V. Oliveira and E. Kraka, J. Phys. Chem. A **121** (49), 9544–9556 (2017).

[117] W. Zou, X. Zhang, H. Dai, H. Yan, D. Cremer and E. Kraka, J. Organometal. Chem. **865**, 114–127 (2018).

[118] E. Kraka, J.A. Larsson and D. Cremer, in *Computational Spectroscopy*, edited by J. Grunenberg (Wiley, New York, 2010), pp. 105–149.

[119] A.D. Becke, J. Chem. Phys. **98**, 5648–5652 (1993).

[120] P.J. Stephens, F.J. Devlin, C.F. Chabalowski and M.J. Frisch, J. Phys. Chem. **98**, 11623–11627 (1994).

[121] R. Ditchfield, W.J. Hehre and J.A. Pople, J. Chem. Phys. **54**, 724–728 (1971).

[122] P.C. Hariharan and J.A. Pople, Theor. Chim. Acta **28** (3), 213–222 (1973).

[123] T. Clark, J. Chandrasekhar, G.W. Spitznagel and P.V.R. Schleyer, J. Comput. Chem. **4** (3), 294–301 (1983).

[124] O. Wiest and K.N. Houk, J. Am. Chem. Soc. **117** (47), 11628–11639 (1995).

[125] S. Marti, V. Moliner, I. Tunon and I.H. Williams, J. Phys. Chem. B **109**, 3707–3710 (2005).

[126] J. Gräfenstein and D. Cremer, J. Chem. Phys. **127** (16), 164113 (2007).

[127] J. Tomasi, B. Mennucci and R. Cammi, Chem. Rev. **105**, 2999–3094 (2005).

[128] J. Jorgensen, W.L. Chandrasekhar, J.D. Madura, R.W. Impey and M.L. Klein, J. Chem. Phys. **79**, 926–935 (1983).

[129] A.M. Nikitin, Y.V. Milchevskiy and A.P. Lyubartsev, J. Mol. Model. **20** (3), 2143–2153 (2014).

[130] A.J. Ranaghan, E. Kara and A.J. Mulholland, Int. Rev. Phys. Chem. **29**, 65–133 (2010).

[131] P. Schwerdtfeger, M. Dolg, W.H.E. Schwarz, G.A. Bowmaker and P.D.W. Boyd, J. Chem. Phys. **91**, 1762–1774 (1989).

[132] D. Andrae, U. Häußermann, M. Dolg, H. Stoll and H. Preuß, Theor. Chim. Acta **77**, 123–141 (1990).

[133] K. Fukui, Acc. Chem. Res. **14** (12), 363–368 (2002).

[134] H.P. Hratchian and E. Kraka, J. Chem. Theory Comput. **9** (3), 1481–1488 (2013).

[135] E. Kraka, W. Zou, M. Filatov, J. Gräfenstein, J. Gauss, Y. He, A. Wu, Z. Konkoli, Z. He and D. Cremer, *COLOGNE18*, Dallas 2018.

[136] M.J. Frisch, G.W. Trucks, H.B. Schlegel, G.E. Scuseria, M.A. Robb, J.R. Cheeseman, G. Scalmani, V. Barone, G.A. Petersson, H. Nakatsuji, X. Li, M. Caricato, A.V. Marenich, J. Bloino, B.G. Janesko, R. Gomperts, B. Mennucci, H.P. Hratchian, J.V. Ortiz, A.F. Izmaylov, J.L. Sonnenberg, D. Williams-Young, F. Ding, F. Lipparini, F. Egidi, J. Goings, B. Peng, A. Petrone, T. Henderson, D. Ranasinghe, V.G. Zakrzewski, J. Gao, N. Rega, G. Zheng, W. Liang, M. Hada, M. Ehara, K. Toyota, R. Fukuda, J. Hasegawa, M. Ishida, T. Nakajima, Y. Honda, O. Kitao, H. Nakai, T. Vreven, K. Throssell, J.A. Montgomery, Jr., J.E. Peralta, F. Ogliaro, M.J. Bearpark, J.J. Heyd, E.N. Brothers, K.N. Kudin, V.N. Staroverov, T.A. Keith, R. Kobayashi, J. Normand, K. Raghavachari, A.P. Rendell, J.C. Burant, S.S. Iyengar, J. Tomasi, M. Cossi, J.M. Millam, M. Klene, C. Adamo, R. Cammi, J.W. Ochterski, R.L. Martin, K. Morokuma, O. Farkas, J.B. Foresman and D.J. Fox, Gaussian 09 Revision D.01 2009 (Gaussian Inc., Wallingford CT).

[137] D.A. Case, I.Y. Ben-Shalom, S.R. Brozell, D.S. Cerutti, T.E. Cheatham, V.W.D. Cruzeiro, T.A. Darden, R.E. Duke, D. Ghoreishi, M.K. Gilson, H. Gohlke, A.W. Goetz, D. Greene, R. Harris, N. Homeyer, S. Izadi, A. Kovalenko, T. Kurtzman, T.S. Lee, S. LeGrand, P. Li, C. Lin, J. Liu, T. Luchko, R. Luo, D.J. Mermelstein, K.M. Merz, Y. Miao, G. Monard, C. Nguyen, H. Nguyen, I. Omelyan, A. Onufriev, F. Pan, R. Qi, D.R. Roe, A. Roitberg, C. Sagui, S. Schott-Verdugo, J. Shen, C.L. Simmerling, J. Smith, R. Salomon-Ferrer, J. Swails, R.C. Walker, J. Wang, H. Wei, R.M. Wolf, X. Wu, L. Xiao, D.M. York and P.A. Kollman, *AMBER 2018* (University of California, San Francisco, 2018).

[138] A.E. Reed, L.A. Curtiss and F. Weinhold, Chem. Rev. **88**, 899–926 (1988).

[139] F. Weinhold and C.R. Landis, *Valency and Bonding: A Natural Bond Orbital Donor-Acceptor Perspective* (Cambridge U. Press, Cambridge, 2003).

[140] M.P. Repasky, C.R.W. Guimaräes, J. Chandrasekhar, J. Tirado-Rives and W.L. Jorgensen, J. Am. Chem. Soc. **125** (22), 6663–6672 (2003).

[141] S.D. Copley and J.R. Knowles, J. Am. Chem. Soc. **109** (16), 5008–5013 (1987).

[142] H.A. Carlson and W.L. Jorgensen, J. Am. Chem. Soc. **118** (35), 8475–8484 (1996).

[143] S. Martí, J. Andrés, V. Moliner, E. Silla, I. Tunón and J. Bertrán, Chem. Eur. J. **9** (4), 984–991 (2003).

[144] J. Giraldo, D. Roche, X. Rovira and J. Serra, FEBS Lett. **580** (9), 2170–2177 (2006).

[145] K. Abdur-Rashid, S.E. Clapham, A. Hadzovic, J.N. Harvey, A.J. Lough and R.H. Morris, J. Am. Chem. Soc. **124** (50), 15104–15118 (2002).

[146] M. Yamakawa, H. Ito and R. Noyori, J. Am. Chem. Soc. **122** (7), 1466–1478 (2000).

[147] D.J. Gustin, P. Mattei, P. Kast, O. Wiest, L. Lee, W.W. Cleland and D. Hilvert, J. Am. Chem. Soc. **121** (8), 1756–1757 (1999).

[148] D. Cremer and J.A. Pople, J. Am. Chem. Soc. **97**, 1354–1358 (1975).

[149] D. Cremer, Isr. J. Chem. **23**, 72–84 (1983).

[150] D. Cremer and K.J. Szabo, in *Conform. Behav. Six-membered Rings*, edited by E. Juaristi (VCH Publishers, Weinheim, 1995), pp. 59–136.

[151] D. Cremer, D. Izotov, W. Zou and E. Kraka, RING Dallas, 2018 < http://www.smu.edu/catco > .

[152] S.D. Copley and J.R. Knowles, J. Am. Chem. Soc. **107** (18), 5306–5308 (1985).

[153] W.J. Guilford, S.D. Copley and J.R. Knowles, J. Am. Chem. Soc. **109** (16), 5013–5019 (1987).

[154] S.D. Copley and J.R. Knowles, J. Am. Chem. Soc. **109** (16), 5008–5013 (1987).

[155] M. Kirsten, J. Rehbein, M. Hiersemann and T. Strassner, J. Org. Chem. **72** (11), 4001–4011 (2007).

[156] C. Uyeda and E.N. Jacobsen, J. Am. Chem. Soc. **130** (29), 9228–9229 (2008).

[157] D.L. Severance and W.L. Jorgensen, J. Am. Chem. Soc. **114** (27), 10966–10968 (1992).

[158] C.J. Cramer and D.G. Truhlar, J. Am. Chem. Soc. **114** (23), 8794–8799 (1992).

[159] D.P. Curran and L.H. Kuo, Tetrahedron Lett. **36** (37), 6647–6650 (1995).

[160] E. Kraka and D. Cremer, Rev. Proc. Quim. **11**, 39–42 (2012).

[161] P. Pyykkö, W. Grochala, C. Stampfl, J. Bernholc, R.D. Hoffmann, R. Pöttgen, T. Fickensher, R. Pöttgen, L.H. Tjeng, V. Honkimäki, X.K. Fang, M.L. Kirk, S. Knottenbelt, P. Kögerler, D.G. Musaev, K. Morokuma, M. Takahashi and C.G. Hill, Chem. Soc. Rev. **37** (9), 1967–1997 (2008).

[162] D.J. Gorin, B.D. Sherry and F.D. Toste, Chem. Rev. **108** (8), 3351–3378 (2008).